From Sensory Detection to Motor Action: The Comprehensive *Drosophila* Taste-Feeding Connectome

Authors
Ibrahim Tastekin[1*#], Inês de Haan Vicente[1#], Rory J. Beresford[1], Billy J. Morris[2], Isabella Beckett[3], Philipp Schlegel[2,3], Marta Costa[2], Gregory SXE Jefferis[2,3], Carlos Ribeiro[1*]

1 Behavior and Metabolism Laboratory, Champalimaud Research, Champalimaud Foundation, Lisbon, Portugal
2 Drosophila Connectomics Group, Department of Zoology, University of Cambridge, Downing Street, Cambridge, UK
3 Neurobiology Division, MRC Laboratory of Molecular Biology, Cambridge, UK

# Authors contributed equally

* Corresponding Authors

Ibrahim.Tastekin@research.fchampalimaud.org

Carlos.Ribeiro@neuro.fchampalimaud.org

Abstract

In *Drosophila*, the gustatory system is distributed across multiple body parts and tightly couples sensory input to value-based behaviors such as feeding, foraging, and social interactions. Despite this, it has remained one of the least mapped sensory modalities at the EM connectome level. Here, we present the first complete wiring diagram of the *Drosophila melanogaster* adult gustatory system, comprehensively reconstructing gustatory receptor neurons (GRNs) from all peripheral organs in a contiguous EM volume spanning brain, cervical connective, and ventral nerve cord. By integrating this male dataset with existing female and male datasets, we generated a pan-CNS, cross-sex connectome, identified GRN types and subtypes via connectivity-based clustering, assigned molecular identities, and uncovered sexually dimorphic circuits. We also mapped all feeding motor neurons and traced how GRN pathways connect to motor and endocrine targets. Using computational approaches, we predicted how sensory input is transformed into feeding, foraging, ingestion, and social behaviors, as well as feedforward neuroendocrine regulation. This defines the action space of the gustatory system and provides a unique framework for understanding how internal states shape taste-driven decisions.

Introduction

Taste is an ancient chemosensory modality that every major animal lineage, from nematodes to insects, fish, and humans, uses to turn the chemical composition of the environment into immediate, value-based actions. By classifying molecules as attractive, neutral, or noxious, gustatory circuits couple detection directly to hard-wired behaviors such as ingestion, rejection, escape, or courtship, thereby steering core survival and fitness decisions in feeding and mating[1,2]. It also conveys important value information which can be used by learning and memory systems to reweight behavior and guide future choices[3,4]. Importantly, gustatory circuits are continuously modulated by internal-state signals, including hunger, satiety, reproductive status, and competing behaviors, so that the very same taste cue can prompt drastically different behaviors depending on the animal's physiological needs[5].

Drosophila melanogaster offers a uniquely tractable system for dissecting both sensorimotor transformations as well as complex behaviors, such as foraging, and how these are modulated by internal state. Its gustatory receptor neurons (GRNs) are molecularly typed, morphologically and behaviorally stereotyped[1,6], and genetically accessible[7–9], yet are embedded in a brain small enough to be reconstructed completely with recent advances in electron microscopy (EM) connectomics, while allowing for complex and sophisticated behaviors. Gustatory pathways are also among the most sexually dimorphic sensory systems in the fly. Several GRN sub-types and their brain targets differ between males and females to bias courtship and sex specific behaviors such as oviposition[4,10]. But a wiring-level comparison of the gustatory system in the two sexes is still lacking. Importantly, in the fly, the recently developed connectome maps[11,12], combined with neurogenetic tools to monitor and manipulate unique neuronal cell types, make it possible to link single identified neurons to feeding, aversion, locomotor, or foraging programs at cellular resolution.

In insects, the impact of taste scales from individual fitness to ecosystems with a strong impact on human wellbeing[13,14]. Adult female mosquitoes, for example, rely on stylet and labellar gustatory neurons to distinguish nectar from blood and to evaluate human skin chemistry, making taste a primary gateway for pathogen transmission[13]. Likewise, the tarsal and palpal sensilla of herbivorous or pollinating insects assess phagostimulants and deterrents on leaves and flowers, determining both crop damage and pollination, which is essential for food security[15,16]. Deciphering the neural logic of gustation in insects thus not only offers a tractable model for understanding gustation at a molecular and circuit level but also eventually manipulating the feeding and host-choice behaviors that underpin agriculture and the spreading of vector-borne diseases.

In most insects, gustatory receptor neurons are not confined to the mouthpart (labellum) but reside in sensilla distributed across different body parts, three groups of pharyngeal sensilla, tarsal and tibial bristles on all six legs, and rows of chemosensory hairs along the wing margin[17,18]. Axons from these anatomically dispersed sensors travel via discrete nerves yet converge onto partially overlapping territories of the sub-esophageal zone (SEZ) and ventral nerve cord (VNC), integrating external sampling, postingestive and internal state feedback, and

reproductive cues within a common circuit framework. At the motor end of this circuit, proboscis muscle motor neurons have been catalogued at single-cell resolution, and SEZ pathways that arrest locomotion upon appetitive taste have been delineated, providing defined behavioral outputs onto which the incoming gustatory tracts must map[19–23]. This distributed architecture broadens the behavioral contexts in which taste can act—during walking, feeding, and mating, for example, and highlights the importance of whole central nervous system reconstructions for a complete understanding of gustatory processing.

EM connectomics has already delivered near-exhaustive wiring diagrams for other *Drosophila* senses: a full inventory of the visual system allows for circuit-level models of motion and color vision[24], while full-brain reconstructions of olfactory and mechanosensory pathways reveal canonical motifs of sensory convergence and descending motor control[25,26]. These resources include the complete adult female brain connectome (FAFB-FlyWire)[12,27,28] and the male ventral-nerve-cord connectome (MANC)[29–31], which together chart brain-to-VNC connectivity at synaptic resolution. In contrast, gustation remains one of the least mapped modalities at the EM connectome level. Only subsets of labellar GRNs have been annotated[32], and the long-range tracts that relay taste to premotor, learning and foraging centers, and their potential sex-specific differences, have yet to be mapped at synaptic resolution in a single, contiguous dataset.

Here we present a pan-central nervous system (CNS) gustatory connectome derived from a contiguous adult male serial-section EM volume that spans brain, cervical connective, and ventral nerve cord. We traced and annotated every gustatory receptor neuron from the labellum, pharyngeal organs, legs, and anterior wing margins and registered them to light-level receptor maps. By cross-matching homologous neuronal cell types from the female brain (FAFB-FlyWire) and the male ventral nerve cord (MANC), we expand this analysis to integrate all available EM datasets, allowing us to assemble a comprehensive and sex-comparable wiring diagram of the fly gustatory system, allowing us to explore sexual dimorphisms in the gustatory system. We then clustered these neurons by fine-scale morphology and by the identity of their downstream synaptic partners, revealing distinct sensory-functional classes that correspond to appetitive, aversive, and pheromonal pathways. The classes converge onto compact second-order hubs that broadcast to proboscis-motor, descending-premotor, locomotor-stop circuits, and neuroendocrine cells, completing the link from detection to defined motor, physiological, and cognitive outputs. This composite dataset closes a major sensory gap in *Drosophila* connectomics and provides a reference for cross-modal computation, targeted perturbation, and ecological applications.

Results

Characterization of the fly's gustatory system at the light level

Since gustatory receptor neurons (GRNs) play a primordial role in *Drosophila melanogaster*'s perception of its chemical environment, these neurons were selected as our entry point to start defining the fly's gustatory connectome. GRNs are housed in sensory organs, named taste sensilla[1]. These structures are distributed through multiple parts of the fly's body, and their morphology differs depending on their exact

location[18,33–37] (Figure 1A). Although very stereotypical in terms of numbers across flies, sexual dimorphisms exist in specific taste sensilla number[33,34]. To map each of the different types of taste sensilla, their location across the body, and sexual dimorphisms, we used different genetic strategies combined with confocal microscopy to label and systematically characterize all GRNs in male and female flies (Figure 1A).

Making direct contact with the external chemical environment, taste bristles are the most numerous and widely dispersed type of taste sensilla. They are thin and long hair-like structures with a pore at their tip, and their numbers vary across body parts, as does the number of GRNs they are innervated by[33–35]. We expressed a nuclear marker (red stinger) together with a membrane marker (mCD8:GFP) using *poxn-GAL4-14*, a driver which had been previously shown to drive expression in all taste bristles[38] (Figure 1A). As described previously, in both sexes, taste bristles are exclusively found on the tarsi and tibia of the flies' six legs, on the anterior margin of the wing, and on the external surface of the labellum (located on the proboscis) (Figure 1A). In general, 30 taste bristles are found on each fly leg, each housing two to four GRNs[6,18,33]. The leg bristle GRNs (lgGRNs) are thought to play a key role in sampling the food in the environment during foraging and suppressing locomotion upon an appetitive response[39]. Male forelegs are an exception, containing, generally, 50 sensilla. The additional bristles on the male forelegs are important for sensing contact pheromones, crucial for courtship behavior[40–42]. On the anterior margin of each male or female wing, 40 taste bristles have been reported, each innervated by four GRNs (Figure 1A). Wing bristle GRNs (wGRNs) have been proposed to play a role in the exploration of ecological niches, especially in the context of sexual behavior[43,44]. Each labial palp of either males or females is reported to be covered by approximately 31 bristles[6,18,34] (Figure 1A). In contrast to other bristles on the body, labellar bristles are unique, as they vary in length and number of GRNs housed depending on their specific localization on the labellum[34]. On the labellum's periphery closest to where the two labial palps meet, there are short(S)- and long(L)-type bristles, which house four GRNs. Occupying a more dorsal area of the labellum's external surface, the intermediate(I)-type bristles are innervated by only two GRNs. The labellar bristle GRNs (lbGRNs) are thought to play a key role in mediating the decision to initiate feeding[17,45].

When flies open their labellum, an event known as labellar abduction or spreading, food becomes accessible to pit-like sensilla, named taste pegs. These anatomically distinct taste sensilla are organized in rows between the pseudotrachea, a distinctive structure on the labellum's inner surface[34], as shown using the *57F03-GAL4* driver, which we have previously demonstrated to specifically label taste peg GRNs (tpGRNs)[46] (Figure 1A). Each taste peg houses a single GRN, and their number is sexually dimorphic, with females having 20% more of these sensilla than males[34] (Figure 1F). In an accompanying paper, we show that a subset of tpGRNs play an important role in controlling the length of a feeding burst towards yeast, by regulating the efficiency of ingestion[47].

Upon ingestion, taste pores lining the pharynx function as internal gustatory sensors. As all GRNs in the pharynx have been reported to express *Ir25a*[37], a broadly expressed gustatory co-receptor, we used *Ir25a-GAL4* to characterize the three specific regions where these hairless sensilla reside (Figure 1A). The labral sensory

organ (LSO), which is composed of nine sensilla, conventionally numbered 1-9, is located ventrally on each side of the midline of the proboscis' haustellum[33,37]. Of those sensilla, only #7-9 house GRNs, with sensillum #7 being innervated by eight GRNs and sensilla #8 and #9 by one GRN each. The ventral cibarial sensory organ (VCSO) and the dorsal cibarial sensory organ (DCSO) are located within the proboscis' rostrum, on each side of the pharynx[37,48]. The VCSO has been reported to comprise either two or three sensilla, housing a total of eight GRNs per side, while the DCSO includes two sensilla per side with three GRNs each. The pharyngeal GRNs (phGRNs) are thought to act as gatekeepers, providing feedback about the quality of the food being ingested and, thus, impacting the decision of accepting and continuing to feed or rejecting it[49,50].

Besides GRNs, taste sensilla often also house one mechanosensory neuron (MSN)[18]. Although being a highly relevant component of the fly's feeding system, we have not included MSNs in the hereby presented connectome analysis.

Description of the GRN projections in the CNS

According to the type of taste sensilla that house them and their localization on the fly body, we classified the GRNs into five broad subclasses, labellar bristle, taste peg, pharyngeal, leg bristle and wing bristle GRNs. Being bipolar sensory neurons, each GRN has a cell body that is located in the periphery, a single dendrite extending towards a pore at the sensillum extremity, through which tastants and other chemicals are sensed, and an axon that projects to specific neuropils in the CNS[48,51]. Because these neurons either terminate and arborize in the SEZ or in the VNC, we grouped the GRN subclasses into SEZ-projecting and VNC-projecting GRNs. To match the projections from the different body parts to the EM data, we first mapped the projection pattern in the CNS of each broad GRN subclass at the light level, followed by manual segmentation of the different projection zones. For this, we used specific GRN-labelling lines for each GRN group. We used *Ir25a-GAL4* driving *UAS-mCD8:GFP* to image the SEZ-projecting GRNs, which include all GRN subclasses, except the wGRNs and a subset of lgGRNs which project to the VNC (Figure 1B). In the SEZ, each GRN subclass projects to discrete regions in the neuropil[51]. phGRNs enter most anteriorly in the SEZ and terminate in regions, including the ventral pharyngeal sensory center 1 (VPS1) and 2 (VPS2), and the posterior maxillary sensory zone 1 (PMS1), which is shared with lbGRNs that also cover other PMS zones[51]. tpGRNs innervate the anterior maxillary sensory zone 1 (AMS1)[51]. Contrary to the other subclasses, lgGRNs either project directly to the SEZ in the brain via the cervical connective, which we named leg ascending GRNs (lgAGRNs) or terminate in the ipsilateral VNC leg neuropils in the first (T1), second (T2) and third (T3) thoracic neuromeres, and we therefore called local leg GRNs (lgLGRNs)[52] (Figure 1C). The lgAGRNs enter the gnathal ganglia (GNG) in the SEZ posteriorly and innervate a region corresponding to the anterior cerebrocervical fascicle (aCCF) terminals, known as aCCFG1[51]. These neurons have very few connections in the VNC. The lgLGRNs are mostly ipsilateral. However, the additional male-specific taste bristles on the male forelegs house bilateral neurons that cross the midline and innervate the leg neuropil on the contralateral side[53] (Figure 1B). The wGRNs terminate in a tightly packed ipsilateral projection in the ovoid, a specialized wing and notum sensory neuropil on each side within T2[35] (Figure 1B).

We also used this light level information together with existing reports[18,33,54] to identify the nerves by which the different GRN classes enter the CNS (Figure 1C). lbGRNs and tpGRNs project through the labial nerve (LbN) from the labellum to the brain. The phGRNs project to the brain via two other mouthpart nerves, the accessory pharyngeal nerve (aPhN), which includes the LSO and VCSO neurons, and the pharyngeal nerve that contains the DCSO neurons. The wGRNs enter the VNC through the anterior dorsal mesothoracic nerve (ADMN) and the lgGRNs via the prothoracic (ProLN), mesothoracic (MesoLN) and metathoracic (MetaLN) nerves, depending if they innervate taste bristles on the fore-, mid- or hindlegs, respectively.

Identification of the GRNs across connectomes

Previous connectomes have covered only part of the CNS, either the brain or the VNC in isolation. As a result, the gustatory system remains one of the last major sensory systems which have not been comprehensively characterized at the EM level. To close this gap, we focused our annotation and characterization effort on a recently generated maleCNS volume, in which the brain and VNC are connected through the neck connective. This dataset gives us complete access to all GRN subclasses across different body parts within one volume (Figure 1C) (Berg et al., 2025 in preparation). Moreover, a substantial fraction of the GRNs' direct downstream partners is descending (DNs) and ascending (ANs) neurons, whose complete form and connectivity are captured in this dataset. To find the GRNs in this volume, we used the available knowledge about the nerves through which GRNs enter the CNS (Figure 1C) to define seed planes through which the axons of different GRNs from each subclass project in a bundle. Neurons were identified as GRNs if their projection field and morphology corresponded to those previously identified in the literature and in our light level maps. We furthermore systematically proofread all the relevant neurons to ensure that the subsequent cell typing was of the highest possible quality. In addition, to avoid missing neurons due to cell segmentation errors, we also employed a complementary approach in which, for each subclass, we identified all the input neurons to the second-order partners of the identified GRNs and reconstructed unidentified upstream bodies that could potentially be poorly reconstructed GRNs, resulting in a comprehensive reconstruction of almost all the GRNs in the maleCNS EM volume (Figure 1C). One of the major limitations of connectomics analysis is the small sample size. Thus, we extended our analysis to two publicly available datasets, the FAFB-FlyWire[12,27,28] and the MANC[29,30] connectomes, respectively, a female brain and a male VNC (Figures 1D and 1E). We completed the existing annotations of every GRN subclass in each volume.

Left–right and cross-dataset counts align closely with one another and with the literature values (Figure 1F). The few discrepancies fall into three clear categories: (i) subclasses with recognized sexual dimorphism, such as the 20% excess tpGRNs in females[34]; (ii) subclasses prone to segmentation artefacts, notably lbGRNs whose thin, densely bundled axons are sometimes falsely split or merged; and (iii) regions of poorer tissue preservation in MANC, specifically of the leg nerves, which likely under-represent lgLGRNs[30]. Based on these data, as well as our light level analysis, we propose that except for the tpGRNs, sexual dimorphisms observed in the connectome counts are likely to result from technical artefacts.

Nevertheless, aside from predictable sexual dimorphisms and these minor segmentation artefacts, all subclass counts differ by only two to three neurons per side across datasets (Figure 1F). One notable exception to the counts in the literature is the wing bristle population: we consistently recover 192-198 wGRNs per side, about 18 % more than the long-standing estimate in the literature (~160 neurons)[18,35]. This upward revision suggests a denser gustatory coverage on the wing than previously appreciated.

Overall, we identified most GRNs across three different connectomes, allowing us to systematically cell type and characterize their downstream circuits. This provides us with the unique opportunity to generate functional hypotheses of how these circuits might initiate, terminate, or sustain foraging, feeding, and other gustatory-driven behaviors.

Cell typing the labellar bristle GRNs

A neuronal cell type can, generally, be defined as a group of neurons which is more similar to neurons in another brain than to any other neurons in the same brain[28]. Our approach to defining cell types was based on clustering our neurons of interest based on their morphology and synaptic connectivity, meaning the neurons they directly connect to, and validating the determined clusters through detailed anatomical inspection and comparison, combined with projection field-based matching. However, to be able to type the GRNs, especially in the maleCNS that was originally mostly untyped, and then, co-cluster the neurons across connectomes, we also had to type their synaptic partners. This was an iterative two-step process that involved grouping the GRN partners using connectivity clustering and assigning a type based on morphologically matching them to neurons in a more comprehensively typed connectome, like FAFB-FlyWire[28,55]. Whenever necessary, the GRN partners were also proofread.

We started by typing lbGRNs as these are the best characterized gustatory neuron subclass in *Drosophila*[10,32,56–59]. We decided to leverage our typing of GRNs in multiple datasets to provide extra robustness to our analysis. Therefore, we used both the lbGRNs we identified in maleCNS (Figures 2A and S1A) and, simultaneously, the corresponding ones in FAFB – FlyWire (Figures 2B and 2C), allowing us to both increase our sampling of neurons by including data from different brains as well as identifying potential sexual dimorphisms. We first clustered male and female lbGRNs separately using cosine similarity scores based on their output connectivity (Figures S1B and S1C), followed by a co-clustering step using both datasets (Figure 2D). Our analysis revealed four broad cell types for the lbGRNs, which we named LB1-4, based on and expanding on a previous cell typing of these neurons using the FAFB – FlyWire dataset[28,32]. The clustering results are supported by clear differences in the overall morphologies of the four types and their consequently distinct projection fields in the SEZ (Figure 2E). Importantly, these features were identical across both connectomes, further strengthening our typing results (Figures S1D and S1E). Upon a complementary detailed inspection of the top downstream partners and the GRN morphologies within each cell type, we further divided LB1-4 into several subtypes (Figures 2E, S1B, and S1C). Each subtype displayed distinct morphological and innervation patterns, which matched between the two connectomes (Figure 2E). Moreover, since the fly brain is mostly

symmetrical, besides matching morphologies on each side (Figure 2E), we also expected each type and subtype to have similar numbers across hemispheres, which is what we observed (Figure 2F). The major differences between hemispheres consisted of four neurons for the LB3d subtype in the maleCNS and eight neurons for the LB3c subtype in FAFB-FlyWire. Furthermore, we could only identify the subtype LB2d in the maleCNS dataset (Figure 2E). While these could represent sexual dimorphisms or inter-individual variability, it is likely that these differences result from poorly reconstructed neurons due to segmentation errors discussed above. As expected from the manual inspection described above, in the co-clustering, the LB1, LB2, and LB4 subtypes clustered together across datasets (Figure 2D). The exception was the LB3 subtypes, which are very likely due to technical challenges with segmenting these neurons. This is supported by the discrepancies observed in the counts of LB3a and LB3d GRNs between the two datasets.

Given the rich available literature on the molecular and functional classes of lbGRNs, we next aimed to assign a receptor identity to as many types and/or subtypes identified in the connectome as possible. The sensing of the chemical environment by GRNs is mediated by specific receptors from three different receptor families, namely ionotropic receptor (IR), gustatory receptor (GR), and pickpocket (ppk) channel families[6,8,9,37,60,61]. Many of these receptors have been linked to sensing either a specific taste modality or particular pheromonal cues and resulting in a particular behavioral output. We therefore generated high-resolution confocal images of the projection patterns of specific *receptor-GAL4* driver lines and matched them to our identified classes.

The LB1a-d neurons project contralateral branches that form an interconnected ring in the midline, with specific variations depending on the subtype (Figure 2E). They best matched the *Gr33a-GAL4* driver projection pattern which is expressed in all bitter-sensing GRNs (Figure 2G). Thus, we propose LB1a-d to be bitter-sensing subtypes that generate aversive responses. While in FAFB – FlyWire these neurons were already annotated as bitter-sensing, our connectivity analysis using the two connectomes suggests that they can be further subdivided into the four proposed subtypes (LB1a-d). This is supported by the earlier observation of the existence of four different functional classes of bitter compound-responsive taste bristles, involving most S- and I-type bristles[56]. Furthermore, L-type bristles were shown not to respond to bitter stimulation or house any GRN expressing bitter-sensing receptors. But recent data suggest that they generate a mild aversive response upon stimulation with specific amino acids like glutamate[10]. This response has been linked to *Ir94e*-expressing GRNs[10] whose projection pattern matches the LB1e GRN morphology (Figure 2E). These neurons are mostly ipsilateral and have a single distinctive dorsolateral branch. While previously assigned a separate type[32], our connectivity analysis across multiple connectomes shows that they cluster together with canonical bitter-sensing GRNs, sharing specific downstream partners. We therefore propose that they are defined as the fifth LB1 subtype, making LB1 a broad aversive type. Using similar lines of reasoning led us to propose that the LB3 type includes appetitive GRNs. The LB3a subtype morphology matched the projection pattern of *ppk28-GAL4* positive neurons, which are supposed to be water-sensing GRNs[62,63] (Figures 2E and 2G). Both LB3b and LB3c projection patterns matched the *Gr64f-GAL4* positive neurons and are, thus, likely to correspond to sweet-

sensing GRNs, mediating appetitive responses[57] (Figures 2E and 2G). Interestingly, the projections of LB3b neurons (Figure 2E) also seem to match the projection pattern of *Ir56b-GAL4* positive labellar GRNs, which have been shown to overlap with GRNs expressing sugar receptors and to be the main mediators of attractive responses to low salt[58,64]. Morphologically, the LB3d GRNs match the glutamatergic *Ir7c-GAL4* and *ppk23-Gal4* positive neurons, which are involved in high salt avoidance responses[59]. The direct downstream connectivity of these neurons overlaps with appetitive subtypes, suggesting that the LB3d aversive GRNs might inhibit the activity of neurons also in attractive circuits via glutamatergic signaling.

Intriguingly, we have not found a *receptor-GAL4* driver line that matched the overall anatomies of the LB2 and LB4 types. Morphology-based comparisons had suggested that the LB2 type is related to LB1e neurons[32] (Figure S1F). However, our connectivity analysis using both connectomes revealed LB2 as a separate type that can be subdivided into LB2a-c with the different subtypes having variations in their outputs and specific anatomies, which are observed across hemispheres in the two datasets (Figures 2D and 2E). Furthermore, our connectivity analysis and detailed anatomical comparisons defined LB4 as a novel GRN type that can be further divided into two subtypes, LB4a and LB4b. Broadly, these neurons are characterized by their mostly ipsilateral projections and a dorsolateral branch. Specifically, LB4a neurons contain anterior branches, while LB4b neurons are, in relation, branching more ventrally and posteriorly (Figure 2E). Existing annotations in FAFB – FlyWire assign LB4a neurons to the LB2 type and LB4b to the LB3 type. Close inspection revealed that especially LB4b neurons differ morphologically from LB3 neurons, as they project more dorsally (Figure S1E). Their overlapping outputs in both connectomes (Figures 2D and S1B and S1C) strengthen the conclusion that LB4a and LB4b neurons belong to the same type. In particular, these neurons share top downstream partners, like AN27X021 or PRW047, which also receive strong inputs from other GRN types from different subclasses.

In conclusion, by combining connectivity-based clustering within and between connectomes, anatomical comparisons, as well as matching with existing known molecular markers, we both identified known lbGRN types and extended the currently available annotations to include new subtypes matching known physiological and behavioral data. Intriguingly, our analysis also revealed a new type, which might represent novel uncharacterized lbGRNs. Computational analysis described later in this paper both supports the functional relevance of this subdivision and also suggests what type of behaviors they might control.

Cell typing the taste peg GRNs

tpGRNs have mostly been regarded as a uniform GRN subclass in the literature[9,34]. Having not been cell typed before at the connectome level, we used an identical strategy to the one described above to type the tpGRNs we identified in the maleCNS and FAFB – FlyWire datasets (Figures 3A, 3B, 3C and S2A). As we also show in a companion paper where we functionally characterize the involvement of these neurons in yeast feeding in female flies[47], tpGRNs consist of two cell types which differ in their morphology and direct downstream connectivity in both male and female brains[47] (Figures 3D, 3E, and S2B). One of the types, which we named dorsal tpGRNs (dtpGRNs), has dorsal projections that are absent in the other type,

which we called claw tpGRNs (ctpGRNs) due to their claw-like projection patterns that are more evident in the FAFB – FlyWire ctpGRNs[47]. It is interesting to note that the anatomies of the two tpGRN types, while broadly matching between the two connectomes (Figure 3C), also have particular variations between the datasets that do not translate into evident connectivity differences (Figure 3D and 3E). This reflects well-known inter-individual variabilities in the detailed projection patterns of gustatory neurons and highlights the advantage of including connectivity-focused analyses in the typing process to reveal functionally relevant cell types. ctpGRNs are the larger population in both datasets, but we only observe a bilateral surplus of ctpGRNs in FAFB – FlyWire (female), whereas dtpGRN counts are identical (Figure 3F). This matches the known female-specific taste peg dimorphism and implies that the extra peg row is innervated exclusively by ctpGRNs[34].

At the molecular level, we propose that dtpGRNs are labeled by *Gr5a-GAL4* and *Ir60d-GAL4*, while ctpGRNs match both *Ir56d-* and *Gr64e-GAL4* projection patterns (Figure 2G). Functionally, we had previously shown that ctpGRNs specifically play a role in sensing carbonation through IR56d[9]. Additionally, this tpGRN type might also be responsive to fatty acids and glycerol, as it is likely to express the glycerol receptor GR64e[65,66]. In a companion paper, we functionally dissect a dtpGRN to a swallowing-controlling proboscis MN pathway that modulates a specific feeding microstructure parameter, the burst length, when amino acid-deprived flies feed on proteinaceous food[47]. Our functional dissection of how these two tpGRN populations control feeding in different ways, together with their distinct receptor profiles and other reported specific roles, are an important experimental validation for the two tpGRN types we have defined at the connectome level.

Cell typing the pharyngeal GRNs

phGRNs have not yet been comprehensively identified and cell typed at the connectome level. To do so, we used the same strategy as described for the other GRN subclasses (Figures 4A-C and S3A). All our connectivity clustering analyses, either with only the maleCNS (Figure S3B), FAFB – FlyWire (Figure S3C), or the co-clustering of phGRNs from both datasets (Figure 4D), suggested the existence of 16 phGRN cell types, which we named PhG1-16. The PhG1 type was the only one we further subdivided into three subtypes, PhG1a-c, based on their specific connectivity and morphology. In contrast to lbGRNs and tpGRNs, phGRNs cell types are generally composed of either one or two right-left pairs of neurons (Figure 4F). It is striking to note that the terminal arborizations of each phGRN type and subtype are unique but mostly preserved in both connectomes and across hemispheres within the same brain (Figure 4E). When we overlay the transformed FAFB – FlyWire phGRN meshes with the maleCNS ones, this morphological conservation can also be seen at the whole population level (Figure 4C). Most phGRN cell types enter the SEZ via the aPhN, coming from either the LSO or the VCSO, and have contralateral projections, except a few types, which are exclusively ipsilateral (Figure 4E). Only PhG7-9 neurons project through the PhN, originating in the DCSO, and all send arborizations across the midline. We propose that a neuron from each of the three types is housed in each of the two DCSO sensilla on either side. This is supported by a detailed receptor-to-neuron map that revealed a mostly unique receptor profile for every phGRN[37]. For the DCSO, previous work showed that each of the three GRNs within a sensillum expresses specific receptors, in a similar arrangement

across both the ventral and dorsal sensilla. Based on the characteristic morphology of one of the mapped DCSO GRNs, we identified PhG9 as corresponding to the GRN labeled by *Ir10a-* and *Ir100a-GAL4* driver[37]. By combining the receptor-to-neuron identification from the literature with our phGRN type matched to *receptor-GAL4* projection patterns, we refined the mapping of GRN types to specific LSO and VCSO sensilla. Here, we have matched *Gr64e-*, *ppk28-*, *Ir67c-, Gr77a-* and *Ir60d-GAL4* driver projection patterns to, respectively, PhG1, PhG3&4, PhG13, PhG15 and PhG16 (Figure 4G). PhG1 should, thus, correspond to neurons in the VCSO and LSO sensillum #7. This latter sensillum should also house PhG13. PhG13 is a particularly interesting type, as we have found it to be potentially sexually dimorphic in its outputs. One of its top partners in the maleCNS is AN05B035, a putative male-specific ascending neuron that innervates the T1 segment of the VNC and projects to the SEZ, sending branches to a region surrounding the esophagus thought to be sexually dimorphic[44,67] (Figure S3D). In females, this phGRN type has been proposed to be involved in a circuit that integrates pheromone and taste information to control receptivity[68]. PhG3&4 should be housed in the LSO and VCSO, while PhG15 and PhG16 should, respectively, correspond to a neuron in VCSO and LSO sensillum#7.

In line with published receptor profiles and our cell typing, the emerging picture is that phGRNs are the most diverse GRN type in terms of morphology and direct downstream connectivity. This diversity supports the idea that these neurons generate unique responses and play unique roles in controlling ingestion.

Cell typing the leg bristle ascending GRNs

Anatomically, leg bristle GRNs can be divided into the ones that directly project to the brain (lgAGRNs) and the ones that arborize locally in the VNC (lgLGRNs) (Figures 1B and 1C). As an intact CNS, the maleCNS dataset has allowed us for the first time to completely reconstruct the lgAGRNs, (Figures 5A, and S4A). We focused our comparative analysis on the FAFB – FlyWire lgAGRNs, given that these include the SEZ terminal arborizations, which capture most of their downstream targets. We identified the SA_VTV_1-5 and SA_VTV_7-10 types in FAFB – FlyWire as corresponding to lgAGRNs (Figures 5B and 5C). Separate clustering of lgAGRNs based on their output connectivity in the female and male connectomes revealed 9 lgAGRN types (LgAG1-9) (Figures S4B and S4D). When we performed the co-clustering of the neurons from both connectomes, the male and female neurons of the corresponding types clustered together, except for one male and one female LgAG4 neuron (Figure 5D). Differences in morphology did not influence their downstream connectivity (Figures 5C and 5E). The counts of each lgAGRN type are comparable between connectomes and hemispheres in the same connectome, with 1 neuron being the biggest difference registered, and LgAG9 (the type with the fewest GRNs), having only one neuron identified in FAFB – FlyWire (Figure 5F).

A great advantage of working in the maleCNS was that we were able to identify from which legs these types project from (Figure S4C). It is interesting to note that 2 types, LgAG1 and LgAG2, are found in all 6 legs. LgAG3, LgAG4, and LgAG8 are the 3 types found only in taste bristles on the mid- and hindlegs. And, the remaining ones, LgAG5, LgAG6, LgAG7, and LgAG9 project mainly from forelegs' taste bristles. Although in previous studies, the expression of specific receptors has been

mapped solely to foreleg GRNs, we could not find reports of receptors being exclusively expressed in mid- and hindleg GRNs[7,69]. Besides responding to fewer compounds, the midleg taste bristles differ in their response when stimulated with the same tastants as their foreleg counterparts[69]. It is therefore possible that the types restricted to mid- and hindleg GRNs do not differ in the receptors they express, but are connected differently to convey, for example, information about the location of gustatory stimuli.

From our effort to attribute molecular identities to these cell types, we have been able to match the *Gr33a-GAL4* driver projection pattern to LgAG1 neurons. This suggests that these GRNs sense aversive compounds, generating an avoidance response[2]. One of its top downstream partners is ANXXX470, better known as TPN3, a neuron which is required for conditioned taste aversion[70]. These neurons are also supposed to express *Gr32a* and sense secreted cuticular hydrocarbons to inhibit conspecific male and interspecies courtship[2,71]. As we observed for PhG13 GRNs, LgAG8 neurons also connect to AN05B035, a potentially male-specific neuron, suggesting, thus, that these neurons have sexually dimorphic outputs and could play important roles in sexual behaviors.

Cell typing the wing bristle GRNs

For VNC-projecting GRNs, like the wGRNs, we compared neurons identified in the maleCNS (Figure 6A) with the corresponding MANC neurons (Figure 6B), allowing us to account for inter-individual differences in the wiring of the male gustatory system. Connectivity clustering using cosine similarity based on the wGRNs' outputs revealed four types, which we named WG1-4 in both datasets (Figures S5A and S5B). The co-clustering of the maleCNS and MANC wGRNs resulted in the clustering of the corresponding maleCNS and MANC types in the same groups, except for WG3 (Figure 6C). In contrast to other GRN subclasses, the different wGRN types are basically formed by the same number of neurons (48-50 GRNs on each side) with minuscule deviations between connectomes and sides (Figure 6E). Morphologically, the different wGRN types are almost indistinguishable from each other (Figure 6D). However, if all the types are overlaid, it is possible to see that they innervate different regions in the neuropil, with WG1 innervating the most anterior area compared to the other types (Figure 6F).

Because the anatomies of the different types are almost identical, we employed a different strategy to propose a molecular identity and, thus, a potential functional role for each type. When possible, we used the top downstream partners of the wGRN types that have been described in the literature to attempt an identification. PPN1, which is annotated as AN05B102a in the maleCNS and as AN_AVLP_20 in FAFB-FlyWire, has been described as a courtship-promoting neuron in males[72]. This neuron is activated by *VGlut+/ fru+/ ppk23+/ ppk25+* GRNs, which have been mapped to project from the wing taste bristles[72]. Likewise, *VGlut-/ fru+/ ppk23+/ ppk25-* GRNs have also been shown to play a role in courtship behavior and exist in equal numbers across the same wing taste bristles[72]. Besides other overlapping outputs, PPN1 is one of the top downstream partners of both the WG3 and WG4 GRN types and since their predicted neurotransmitter is, respectively, glutamate and acetylcholine in both connectomes, we propose that WG3 correspond to the *VGlut+/ fru+/ ppk23+/ ppk25+* GRNs and WG4 to the *VGlut-/ fru+/ ppk23+/ ppk25-* GRNs. A

different set of wGRNs, which also plays a role in courtship behavior, has been demonstrated to express *fruitless* and *IR52a*, with some neurons also expressing *IR52b*[44,67]. Trans-Tango-based circuit tracing using both *Ir52a*- and *Ir52b-GAL4* has revealed that directly downstream of these GRNs, only in the male brain, there are neurons that have projections around the esophagus, which have been described to be sexually dimorphic[44,67]. Besides WG3 and WG4, only the WG1 GRN type has those kind of sexually dimorphic neurons as relevant partners (Figure S6A), leading us to propose that these GRNs are the previously identified courtship-promoting *fru+/ Ir52a*+ GRNs[44,67]. Moreover, the literature suggests that wGRNs express sugar GRs, like *Gr43a*, *Gr64f,* and *Gr5a,* and respond to sugar stimuli[39,43,73,74]. A key downstream partner of WG2 is Dandelion, an AN typed as AN13B002 in the maleCNS and as AN_GNG_68 in FAFB-FlyWire. Given that Dandelion is also a key downstream neuron of LB3b GRNs in the labellum, which we also propose to express sugar GRs, we propose that the WG2 GRNs are likely to detect sugar and trigger feeding. This approach of using key shared downstream partners to assign shared functions across the connectome therefore, emerges as an important strategy to propose similar functional roles to different GRN cell types across multiple subclasses. A strategy we will employ more comprehensively in later analyses.

A last important observation is that all the defined male wGRN types connect strongly to specific second-order neurons, which are morphologically different between maleCNS and FAFB – FlyWire and, thus, are likely to be sexually dimorphic (Figure S6A). AN05B102d and ANXXX151 (matching, respectively, AN_multi_69 and AN_multi_71 in FAFB-FlyWire), two AN types that are directly downstream of WG1 have projections around the esophagus, a region that has been suggested to be sexually dimorphic in males[44,67]. The same occurs for another output AN of WG3 and WG4 GRNs, annotated as AN05B102c in the maleCNS and AN_AVLP_PVLP_5 in FAFB-FlyWire. The WG2 GRNs connect to ANXXX013, which has been matched to AN_GNG_150 in FAFB – FlyWire and has an extended dorsal projection in the maleCNS brain outside the SEZ. Taken together, these analyses therefore reinforce the idea that wGRNs are sexually dimorphic in terms of their downstream connectivity and play a key role in mediating sexually dimorphic social behaviors in flies.

Cell typing the leg bristle local GRNs

Similar to the wGRNs, to cell type the lgLGRNs we used the neurons identified in maleCNS (Figure 6A) and MANC (Figure 6B). Because these neurons span the T1-3 segments of the VNC, we did the connectivity clustering separately for each pair of front-, mid-, and hindlegs, which project to T1, T2, and T3, respectively. From the co-clustering of maleCNS and MANC lgLGRNs, we defined 4 types, LgLG1-4, which are found across all legs (Figures 6G, S5C, and S5E). All the GRNs from these types have ipsilateral projections, terminating within the leg neuropil on the same side that they enter the VNC. Each of the 4 types has a characteristic morphology at the population level, arborizing in different regions of the neuropil (Figures 6H and S5G). The morphology of LgLG4 GRNs is the most distinct from the 4 types. The LgLG1 type is the only type we have further subtyped. Given that they are predicted to release different neurotransmitters, we divided LgLG1 into LgLG1a and LgLG1b, respectively, depending if the GRN is predicted to express acetylcholine or

glutamate (Figures 6G, S5C, and S5E). Considering their morphology, LgLG1a and LgLG1b seem to overlap in the same regions in the leg neuropils (Figure S5G). In terms of GRN counts in both connectomes, LgLG1 is the type with the most neurons, while LgLG4 is the type with the fewest GRNs across the fore-, mid-, and hindlegs (Figures 6J, S5D, and S5F). An observation regarding MANC is that there seems to be an overestimation of LgLG1b GRNs compared to LgLG1a, if we consider that the numbers of the two subtypes are essentially the same in maleCNS.

To assign a molecular identity to these lgLGRN types, we once more used top downstream partners that have been described in the literature and associated with GRNs expressing specific receptors and playing determined behavioral roles. Equal to the WG3 and WG4 types, LgLG1 GRNs also have PPN1 as their top downstream partner. Since both *VGlut-/ fru+/ ppk23+/ ppk25-* and *VGlut+/ fru+/ ppk23+/ ppk25+* GRNs have been mapped to leg taste bristles[72], we propose that those molecular identities correspond to the LgLG1a and LgLG1b types. Similar to WG1 GRNs, the LgLG2 type has output neurons that extend projections to the sexually dimorphic region around the esophagus, and since *IR52a* and *IR52b* have been mapped to the same lgLGRNs, we propose that LgLG2 corresponds to *fru+/ Ir52a+/ Ir52b+* GRNs[42]. Similar to WG2, LgLG3 GRNs have Dandelion as one of their top downstream partners. We therefore propose that it is likely to express sugar GRs, especially *Gr5a*, which is expressed by lgLGRNs[74]. LgLG4 also has Dandelion as a relevant second-order neuron, and it shares other appetitive outputs, like DNg103, with other GRN types. The anatomy of these neurons matches published projection patterns of sugar *Gr-GAL4* driver lines, leading us to propose that LgLG4 are likely to mediate appetitive sugar responses[4].

The co-clustering of lgLGRNs from the two connectomes revealed 4 additional cell types, LgLG5-8, which project exclusively from the forelegs to T1 (Figures 6G, S5C, and S5E). The neurons comprising these types have mostly contralateral projections, crossing the midline and innervating the neuropil on the opposite side of their entrance into the VNC (Figure 6H). It is well known that these contralaterally projecting neurons are sexually dimorphic, projecting from taste bristles that exist solely in males[72]. They have been shown to play a role in contact pheromone sensation. The counts of these types are very comparable across both connectomes and between both sides of the same VNC (Figure 6J). In the maleCNS, the predicted neurotransmitter for the LgLG5 and LgLG8 GRNs is glutamate, while for the LgLG6 and LgLG7 GRNs it is acetylcholine (Figure 6G). However, in MANC, all 4 types are predicted to express glutamate. Assuming there is some bias towards glutamate when predicting the neurotransmitter in MANC neurons, we propose LgLG5 and LgLG8 to be *VGlut+/ fru+/ ppk23+/ ppk25+* GRNs and LgLG6 and LgLG7 to be *VGlut-/ fru+/ ppk23+/ ppk25-* GRNs. Contralateral GRN populations with either one of those molecular identities have been previously shown to exist in males[72]. Interestingly, PPN1 is not a relevant second-order neuron of any of these cell types. However, many of their downstream partners are male-specific or sexually-dimorphic ANs (Figure S6B), supporting our proposal that these are male-specific pheromone-sensing neurons, mediating sexually dimorphic social behaviors.

Taken together, our cell typing effort of GRNs across three connectomes has allowed us to both identify known GRN types previously described using molecular, anatomical, physiological, and behavioral approaches, and to expand their

classification into functionally relevant new cell types, as exemplified by a separate paper focusing on tpGRNs[47]. We also characterize inter-individual differences across datasets, as well as known sexual dimorphisms. Thus, our GRN cell typing should represent the first comprehensive annotation and characterization of the gustatory system in any insect. This provides a unique opportunity to further explore the circuit basis of how these GRNs might mediate specific behaviors.

Functional organization of the gustatory connectome

Activities of GRNs across different body parts should be integrated in downstream circuits to orchestrate the actions underlying complex feeding decisions[17]. During foraging, leg bristle GRNs slow locomotion upon food encounters and trigger proboscis extension to probe food quality together with labellar bristle GRNs. If the food is appetitive, the fly stops and extends its proboscis. Labellar bristle and taste peg GRNs get sequentially activated by food, while the swallowed nutrients are monitored by pharyngeal sensilla. To study GRN populations that converge on similar downstream circuits, and therefore likely encode similar valence and/or mediate similar behaviors, we performed UMAP embedding of the SEZ-projecting GRNs in maleCNS and FAFB – FlyWire based on their immediate downstream connectivity (Figure 7A). Importantly, we included only the monomorphic second-order neurons to focus on common pathways in both sexes (Figure 7A). Including dimorphic neurons did not change the clustering, as the number of dimorphic partners is much lower than the monomorphic partners in general (data not shown, Berg et al., 2025, in preparation). Our UMAP embedding clustered GRNs of the same type from both datasets together, validating both our cell typing as well as the clustering.

Our UMAP analysis revealed 8 main clusters. One of the main clusters contains the bitter-sensing LB1 subtypes (Figure 2), and we therefore decided to name it the aversive cluster. It also contains several phGRN types (PhG3-7, 9, 11, 13, 14, 15, and 16) and lgAGRN types (LgAG3, LgAG5, and LgAG8) (Figures 7A and S7A). As the pharynx is an important checkpoint for assessing food quality before the passage into the digestive system, we propose that these phGRN types are important for limiting food intake. Indeed, it has been shown that different combinations of phGRNs are required to suppress food intake and avoid bitter compounds[75]. Functional studies dissecting the common circuitry downstream of the aversive PhGs will be important to unravel the mechanisms of the combinatorial logic underlying pharyngeal sensorimotor transformations. While we could not assign a function to the LB2a-d types based on known receptor expressions, these can be found in this cluster, suggesting that they might mediate aversion responses. Interestingly, despite having sexually dimorphic outputs, PhG13 GRNs from both males and females are also found in this cluster. We propose that, similar to LgAG1s[2,71], IR67c positive neurons might contribute to avoiding ingesting bitter compounds as well as regulating sexual behavior.

We deduced that another major cluster must contain GRNs mediating attractive behaviors, as it encompasses all LB3 GRNs, which we proposed to correspond to sugar and other phagostimulatory GRNs (Figures 2, 7A, and S7B). LB4a and b, which we could not assign a molecular identity, are also in this cluster, suggesting that they might convey attractive information too (Figure S7B). Two pharyngeal GRN

types, PhG1 (including all subtypes) and PhG10, are also in this attractive cluster. This agrees with our receptor-GAL4 matching, suggesting that PhG1s express Gr64e (Figure 4G), which is important for detecting glycerol and fatty acid and inducing proboscis extension towards these stimuli[2,37,65].

LgAGs 4, 7 and 9, and PhG12 comprise another cluster. Although we cannot assign a clear role for this cluster, we propose that these GRNs also mediate aversive responses, as they share GNG016 as a downstream partner with GRNs in the other major aversive cluster.

ctpGRNs and LgAG6 form a unique cluster with unknown behavioral relevance. Likewise, PhG2, PhG8, and dtpGRNs also form a separate cluster. In an accompanying paper, we show that dtpGRNs anticipatorily facilitate ingestion to increase the length of yeast feeding bursts and therefore protein intake[47]. Finally, LgAG1 GRNs from both maleCNS and the FAFB – FlyWire datasets form a unique cluster. As we mentioned above, this GRN type is important for sexual behavior in *Drosophila* as well as aversive responses.

Because these clusters arise from GRNs that converge onto common downstream neurons, they provide a unique entry point for predicting the functional logic of the circuits and behavioral programs they underlie. GRNs from the major aversive clusters, as well as LgAG1, which was shown to be important for avoidance[2], synapse with GNG016 (Figures 7B and 7C). Of note, GNG016 is predicted to be a GABAergic neuron, and it has feedback connections with the aversive GRNs it receives inputs from (Figure S8A). This feedback mechanism could, for example, serve as gain control, sharpening signals, or creating oscillations. The functional relevance can only be answered with careful functional dissections. GNG016 signals to GNG510 (Figures 7C and S8B), which outputs onto GNG087 (Scapula) (Figures 7C and S8C). Interestingly, Scapula was proposed to inhibit proboscis extension by directly suppressing the activity of a premotor neuron[45]. GNG510 also connects to GNG088 (Figures S8C and S8E), a GABAergic neuron that we predict to directly inhibit proboscis motor neurons that are involved in pharyngeal pumping (Figures 7C, 8, and S8F). Interestingly, GNG510 receives direct inputs from GRNs from both aversive clusters, including LB2b, LB2c, LgAG7, and LgAG9 (Figures 7C and S8B). Moreover, Scapula also receives direct inputs from another aversive GRN type, LB1c, demonstrating that the aversion circuits receive GRN inputs across multiple layers. Together, this circuit suggests that aversive gustatory cues are likely to suppress feeding by inhibiting proboscis extension and food swallowing.

This aversive circuit is not unique, as other parallel circuits inhibiting feeding can be identified. A good example is the circuit downstream of PhG2 (Figure 7E). GNG055 receives strong inputs from PhG2 and LB1c and is predicted to inhibit Fdg (GNG588), which has been previously shown to be an important neuron coordinating feeding and halting forward locomotion[21,45,76]. Therefore, our findings suggest that aversive GRNs suppress feeding at different, parallel levels (Figure 7F). They influence specific downstream neurons that inhibit feeding at different levels of the sensorimotor arc, ranging from higher-order to premotor to motor neurons.

Given its importance for modulating social behavior, we also inspected the LgAG1 cluster (Figure 7A). AN05B023a, a GABAergic neuron downstream of LgAG1

(Figures 7G and 7H), and LgAG1 are each other's top reciprocal synaptic partners. AN05B023a, in turn, inhibits PPN1 (AN05B102a), a neuron known to promote courtship[72]. Since *Gr32a*+ LgAG1 neurons have been shown to suppress interspecies and male-male courtship[2,71], we propose that they do so by inhibiting PPN1 (Figure 7H). Surprisingly, male-female courtship-promoting, *fru+/Ir52a*+ WG1 and LgLG2 GRNs are also strong upstream partners of AN05B023a (Figures 7G and 7H). Dissecting how AN05B023a integrates pheromone inputs from different GRN types will be key to understanding its role in controlling courtship behavior.

To sum up, our UMAP analysis confirms our initial clustering and expands our initial functional cell typing, allowing us to predict the valence of the recognized stimuli. Our analysis also suggests that activity of GRN types from different body parts is integrated by common downstream partners based on valence (attractive vs. aversive) to control and coordinate specific behavioral outputs (feeding, sexual behavior, ingestion). By mapping key second-order neurons downstream of different functional clusters to different actions such as feeding aversion and courtship inhibition, we uncovered circuit architectures that can integrate inputs from different GRN types to coordinate flexible actions. This creates strong predictions that can be directly tested with the available genetic tools.

Characterization of SEZ motor outputs from the GRN cell types

While the UMAP approach allows us to make broad predictions of the functional relevance of GRNs on behavior, these are inferred from the known function of specific interneurons. A detailed understanding of behavior requires the detailed mapping of the sensory-motor arc from sensory neurons to unique motor neurons innervating specific muscles. One of the main roles of gustatory systems is to guide feeding behavior. Specific motor neurons (MNs) mediate stereotyped motor responses upon the activation of the corresponding sensory system, which, when appropriately coordinated, lead to specific behavioral outputs. Similar to almost all GRN subclasses, all MNs mediating the feeding behavior of the fly are also localized in the SEZ, making this neuropil the key brain region which implements feeding-relevant sensorimotor transformations[47,77,78]. To link GRN cell types to different behavioral outputs, we identified and cell typed all SEZ motor neurons in the maleCNS and FAFB – FlyWire datasets.

The feeding MNs have their cell bodies located in the brain, and exhibit characteristic branching patterns in the SEZ[19,22,23]. Their axon exits the brain via one of the two ipsilateral mouthpart nerves, the PhN or the LbN. To identify the neurons in the maleCNS dataset (Figure 8A), we searched for morphological matches to all the MNs exiting through the PhN and the LbN in FAFB – FlyWire (Figure 8B). Whenever a match was not found, we used the previously described seed plane strategy to find and proofread the MNs. Validating our identification in maleCNS, we found matching cell number counts for the MNs exiting via the LbN between hemispheres and to FAFB – FlyWire (Figure 8C). For the MNs exiting the PhN, we observed differences across the right and left sides within maleCNS, similarly to what was annotated in FAFB-FlyWire, and between the two connectomes. This might either correspond to inter-individual variabilities or challenges in the reconstruction and identification of the missing neurons.

Similar to the strategy used for the GRNs, we used connectivity clustering based on cosine similarity of the MN inputs to define different feeding MN cell types. We furthermore visually inspected and compared the corresponding morphologies of the neurons in each cluster to validate that they were correctly matched. The resulting separate connectivity clustering of maleCNS (Figure S9A) and FAFB – FlyWire feeding MNs (Figure S9B) allowed us to identify 24 different cell types. Importantly, the co-clustering of the MNs from both connectomes revealed the same 24 types, with the corresponding male and female neurons clustering together (Figure 8D). Only one maleCNS MN, typed MN11D, and one FAFB – FlyWire MN, annotated as MN11V, did not cluster with their types. In the case of the maleCNS MN, this is very likely due to an incomplete reconstruction of the neuron.

To assign the identified MN cell types to different muscles and therefore functional classes, we took advantage of detailed previous work done on feeding MNs identification and characterization at the light microscopy level[19,20,22,23,79]. Most feeding MNs innervate muscles in the proboscis and are, thus, globally known as proboscis MNs. The fly's proboscis is a segmented appendage formed by the labellum, haustellum, and rostrum (Figure 8E), which are individually controlled and sequentially moved through specific joints to contact food[19,22,23]. Feeding MNs can be categorized into five groups depending on their overall role. (i) Proboscis MNs 1, 2D, 2V, 3M, 3L, 4, 6, and 9 have been shown to control different steps of proboscis positioning, which includes the extension of its different segments, upon stimulation of appetitive gustatory GRNs (Figures 8E and S10). (ii) Proboscis MNs 7 and 8 mediate labellar opening or spreading, upon an attractive stimulus. (iii) Proboscis MNs 11D and 12D have been shown to control pharyngeal pumping[21,47,80], allowing the food to reach the esophagus. Given that they target muscles around the pharynx, MNs 5, 10, 11V, and 12V have been proposed to have similar functions in pharyngeal pumping (Figure 8E and S10). (iv) Proboscis MN13 is predicted to play a role in controlling salivation as the muscle it innervates inserts at the junction of the salivary duct with the pharynx[23] (Figure 8E and S10). MN12V[23] was the only proboscis MN for which no anatomical match was found in either maleCNS or FAFB-FlyWire. It is also important to note that we also identified MN2D- and MN4-like neurons, which we have typed as MN2Db and MN4b, respectively. These types have similar upstream connectivity to the originally identified MNs 2D and 4, annotated, respectively, as MN2Da and MN4a, and morphologies similar enough to resemble those neurons but sufficiently different to be their own type (Figure 8D and S9C). (v) Another feeding MN, CEM, which innervates muscles at the crop entrance, has been shown to have a role in the postingestive decision to let food pass to the crop or not[79] (Figure 8F). Previously identified in FAFB-FlyWire, we also found CEM in the maleCNS dataset (Figure 8D and S9C). Furthermore, in both datasets, we identified 5 MN types, named MNx01-05, (Figure 8D), that, to our knowledge, have never been described in the literature. Anatomically, each MN cell type is distinct, but identifiable across connectomes (Figure S9C). Some project ipsilaterally like MN2Da, MN7, MNx04, and MNx05, while most are bilateral. In general, as previously reported, SEZ MNs are either one or two right-left pairs of neurons (Figure S9D).

This functional specialization is also reflected in the connectivity clustering, revealed by three main clusters (Figure 8D). The first cluster is formed by MNs that are involved in the movement of the proboscis parts such as positioning of rostrum and

haustellum as well as spreading of the labellum[19,22,23]. The second cluster is mainly formed by MNs involved in pharyngeal pumping[19,23] and the third cluster is formed by the CEM neurons controlling crop entry[79]. This finding suggests that MNs form functional units each of which are controlled by common premotor circuits to coordinate proboscis positioning and ingestion.

Characterization of Sensorimotor Pathways Controlling Feeding Motor Actions

Because the EM datasets contain all GRNs, feeding MNs, descending interneurons controlling locomotion, and other relevant neurons in the, we are uniquely positioned to map how sensory information is transformed into actions. Taste is especially well-suited for this analysis, as taste-evoked behaviors are largely hard-wired. To do so, we used a strategy relying on calculating the effective connectivity scores between different GRN – effector neuron (e.g. MN) type pairs (see Methods)[65]. Effective connectivity is an inferred estimate of how strongly activity in a given GRN type could influence an MN, considering not only direct synaptic connections but also indirect routes through intervening neurons. Importantly, it normalizes synaptic weights by the total input into target neurons at each layer. In this sense, it is analogous to evaluating synaptic drive in a physiological experiment: strong direct inputs contribute heavily, while longer multi-synaptic paths (numbered as hops) contribute progressively less. The metric thus captures the cumulative potential impact of a sensory input on a motor output across the polysynaptic network. As the maximum number of neurons a GRN can reach over multiple hops plateaus at 6-7 hops, we started by calculating the effective connectivity of each GRN-MN pair for up to 7 hops (Figures S11 and S12). High effective connectivity scores indicate that GRNs influence specific MNs strongly.

Hierarchical clustering of effective connective scores between lbGRN – MN pairs led to two main clusters of lbGRNs in the maleCNS dataset (Figure S11A). The first cluster is formed by the attractive lbGRNs, LB3a-d, and the aversive LB1a. These GRNs have relatively high effective connectivity scores with MN types that are involved in proboscis positioning and labellar spreading. This observation is consistent with the large body of knowledge showing that activation of phagostimulatory lbGRNs such as Gr64e is sufficient to trigger proboscis extension. Interestingly, the second cluster, which is formed by LB1b, c, d, e, LB2s, and LB4s, has very low effective connectivity scores with proboscis positioning MNs. In contrast, these neurons are predicted to be strongly connected to MNs that control pharyngeal pumping and crop entry. As our cell typing and the UMAP analysis suggest that LB2s mediate aversion and LB4s mediate attraction, we propose that LB2s do so by suppressing the ingestion of aversive compounds while LB4s promote ingestion. LB2s have particularly high effective connectivity scores with CEM neurons, which have been suggested to control food passage in the fly digestive system. We therefore propose that the control of food passage in the digestive system might be an important function of LB2s. Importantly, clustering functional connectivity scores using the FAFB – FlyWire dataset led to similar results, with only small differences in some subclusters (Figure S11A).

Another way to dissect how GRNs affect feeding behavior is to compute which MNs they reach with the least number of hops. We therefore computed the effective

connectivity scores between GRN – MN pairs at each hop and ranked them according to which reached the corresponding MNs with the least number of hops (Figure S11B). We focused on MNs that are key for controlling different steps of feeding: MN9 (rostrum protraction), MN4a (haustellum extension), MN6 (labellar extension), MN8 (labellar abduction/spreading), MN11D or V (pharyngeal pumping), and CEM (crop entry). LB3a-d (sugar and other phagostimulatory GRNs) and LB1a (bitter GRN) reach maximum effective connectivity scores with proboscis positioning and labellar spreading MNs after 4-5 hops. In addition, they show a sharp increase in effective connectivity score already after 2-3 hops (Figure S11B). While it is at first sight counterintuitive that bitter and sugar GRNs are predicted to reach proboscis positioning MNs with the same effectiveness, this agrees with the previous findings that aversive GRNs mediate aversion via suppressing feeding-promoting sensorimotor pathways and not by acting on other MNs, such as the ones mediating proboscis retraction. Similar to what we observed in the previous analysis, LB2 GRNs reach high effective connectivity scores with pharyngeal pumping MNs and CEMs in fewer hops than other GRN types. This strongly suggests that they are important for modulating ingestive and postingestive behaviors. These findings suggest that proboscis extension and ingestion are mediated by a multilayered circuitry, which allows for the implementation of complex feedforward and feedback regulatory mechanisms.

We applied the same approach to tpGRNs and phGRNs. As we report in an accompanying paper, dtpGRNs have strong connections with pharyngeal pumping MNs as well as the CEM neurons[47]. ctpGRNs exhibit interesting dimorphisms between the two datasets (Figure S12A). While they are strongly connected to proboscis positioning MNs in the male dataset, they are more strongly connected to pharyngeal pumping MNs in the female dataset. As we identified genetic driver lines labeling this GRN type, further functional dissection will clarify the functional relevance of this potential sexual dimorphism. Interestingly, ctpGRNs reach high effective connectivity scores with proboscis positioning MNs in fewer hops when compared to dtpGRNs. dtpGRNs and ctpGRNs have similar profiles for MN11V. However, dtpGRNs reach CEMs in a few hops and have comparably high effective connectivity scores with these MNs (Figure S12B).

phGRNs seem to be poorly connected to proboscis positioning MNs except for PhG2. In general, phGRNs are strongly connected to pharyngeal pumping MNs and CEM (Figure S12C). This supports the idea that the main function of phGRNs is to control food passage to the digestive system and to therefore, serve as gatekeepers of the body. Something, which is not surprising given their anatomical location.

As stated, PhG2 reaches high effective connectivity scores with proboscis positioning and pharyngeal pumping MNs after 3-4 hops (Figure S12D). Most phGRNs reach high effective connectivity scores with MN11V in few hops, with PhG2 having the highest score. As previously mentioned, PhG2 is likely to inhibit proboscis extension and ingestion[21] by suppressing different MNs (Figure 7E), explaining why it is connected to all feeding-relevant MNs. Finally, PhG3, PhG4, PhG6, and PhG7 reach high effective connectivity scores with CEM in only 4 hops (Figure S12D). As we proposed earlier, PhG3 and 4 are likely to be *ppk28*+, water-sensing phGRNs. This observation suggests that water entry to the crop is tightly regulated by these phGRNs. Intriguingly, PhG12-14 and PhG16 seem to be weakly

connected to any feeding or ingestion MN when compared to other phGRNs in the maleCNS (Figures S12C and S12D), suggesting that they might instruct other behaviors like maybe learning and memory. In FAFB – FlyWire, PhG15 also joins this cluster, while being strongly connected to CEMs in the maleCNS (Figure S12C).

To reconstruct a minimal sensorimotor circuit that connects attractive lbGRNs LB3a-d to proboscis positioning motor neurons (MNs 9, 6, 4 and 8) as well as LB2s to CEMs we selected neurons with high effective connectivity scores with both GRNs and MNs at each hop (Figures 8G and 8H; see Methods). This analysis revealed key second-order, higher-order and premotor neuron types, some of which have already been identified as controlling feeding in other studies, suggesting that our approach extracts important circuit features underlying behavior[47]. Careful dissection of these sensorimotor pathways revealed two distinct circuit motifs which could be observed multiple times across the feeding circuit. First, we observed a three-hop motif which leads to the disinhibition of different MNs controlling proboscis positioning and crop entry (Figure 8I). In one example, the activation of the GABAergic second-order neuron Quasimodo by phagostimulatory GRNs leads to the disinhibition of MNs9, 4a, and 8, therefore enabling them to get activated (Figure 8I). Second, we observed a longer, four-hop feedforward excitation pathway mediated by the key cholinergic second-order neuron Clavicle (ANXXX462), which should lead to the activation of the same MNs (Figure 8J). We propose that the temporal dynamics produced by the combination of three-hop disinhibition and four-hop feedforward excitation might allow for the generation of complex rhythmic proboscis extension and retraction cycles, such as observed when the fly feeds on solid food[81]. We furthermore observed a four-hop incoherent feedforward circuit controlling the CEM neurons via the cholinergic Doublescoop and glutamatergic CB0041 neurons (Figure 8K). As genetic driver lines labeling these cell types exist[35], it will be possible to dissect the circuit dynamics controlling crop entry by labellar bristle inputs.

Taken together, our analysis suggests that each step of the motor sequence underlying fly feeding is controlled by a group of specific GRNs that are distributed across different taste sensilla.

Feedforward Control of Neuromodulation by GRNs

One of the most striking consequences of taste is its ability to modulate peripheral physiology before nutrients are absorbed into the body. In mammals, this is exemplified by the cephalic phase insulin response (CPIR), where food-related sensory signals activate parasympathetic pathways to trigger insulin secretion in advance of food digestion. Beyond insulin, food perception is sufficient to modulate the activity of brain regions that regulate satiety states[82–84] and to impact peripheral metabolism, including hepatic homeostasis[85], lipolysis[86], and adipose tissue thermogenesis[87]. We therefore asked to what extent GRNs are wired into neuroendocrine circuits that prepare the organism for metabolic challenges. Given that neurosecretory cells (NSCs) that produce various hormones have been identified in the FAFB – FlyWire and maleCNS datasets[88] (Berg et al., 2025, in preparation), we computed effective connectivity scores between maleCNS GRNs and NSCs predicted to express insulin (labeled as IPCs), hugin (labeled as Hugin neurons), ion transport peptide (labeled as ITP neurons), CAPA (labeled as CAPA neurons), diuretic hormone 31 (labeled as DH31 neurons), diuretic hormone 44

(labeled as DH44 neurons), corazonin (labeled as CRZ neurons), or myosuppressin (labeled as DMS neurons) (Figure S13A). One cluster comprising most phGRN types, dtpGRNs, and the labellar LB2 and LB4 types had particularly high connectivity scores with DMS, DH44 and IPC neurosecretory neurons (Figure S13A). Interestingly, these GRNs also have high effective connectivity with MNs that control pharyngeal pumping and ingestion (Figures S11 and S12). Other GRNs, especially lgGRNs and wGRNs, showed generally low effective connectivity with NSCs (Figure S13A). This makes sense, as simple food sampling via leg and wing bristles, without ingestion, should not lead to an anticipatory remodeling of animal physiology. Similarly, LgAG1 neurons, which we predict are involved in sexual behavior, are also in this cluster.

Our findings suggest that taste perception and neuronal signaling at early stages of ingestion might prime metabolic programs for satiety, like in mammals[89]. To start dissecting the neuronal circuits doing so, we focused on the connectivity of putative sugar-sensing PhG1s with insulin-secreting IPCs. Our circuit reconstruction shows that PhG1a-c connect to IPC in three hops through a layered, convergent feed-forward relay (Figure S13B). Interestingly, CB0041 and the Sustain neuron, which are involved in controlling the length of yeast feeding bursts[47], connect phGRN types to IPCs. The involvement of Sustain and CB0041 suggests that the same interneurons that control feeding burst length may also couple ingestion to IPC activity, linking microstructure of feeding with systemic metabolic regulation.

Control of Proboscis Motor Neurons by Leg and Wing GRNs

Foraging flies detect food first using their bristle sensilla on each of the six legs before they extend their proboscis, showing that food detection by leg GRNs is sufficient to trigger proboscis extension[22]. To identify candidate circuits that transform appetitive stimulation of appendages into proboscis movements, we decided to compute the effective connectivity scores between leg and wing bristle GRNs and feeding motor neurons. We normalized the scores by the total leg/wing GRN scores to highlight the relative connection of each GRN type to each MN (Figure 9A). Our analysis showed that wGRNs and lgGRNs are poorly connected to feeding MNs except for the LgLG4 type, which is included in the cluster that is more strongly connected to feeding MNs. The GRN types we proposed to be appetitive, LgAG2 and LgLG4 (Figures 6H and 7A), are clustered together (Figure 9A), suggesting that their activity is integrated to generate proboscis extension response to appetitive stimuli. To predict which leg GRN types exert the most direct influence on feeding motor neurons, we calculated effective connectivity scores and identified those reaching the highest scores with distinct feeding motor neurons in the fewest hops. Among them, LgLG4 stands out, reaching high connectivity scores after few hops with each of the motor neurons controlling the entire feeding motor sequence: MN9 (rostrum protraction), MN4a (haustellum extension), MN6 (labellar extension), MN8 (labellar spread), MN11D (pharyngeal pumping) and CEM (crop entry) (Figure S14A). On average, however, LgLG4 requires 7 hops to reach its maximum effective connectivity score with feeding MNs, two more than most labellar GRNs. This fits with the well-known observation that labellar gustatory stimulation is more efficient in eliciting proboscis extension than leg stimulation.

Careful analysis of the LgLG4 downstream circuits revealed that LgLG4 connects to Bract neurons in two hops via the ascending neuron AN01B004 (Figure 9B). Bract neurons are also downstream of labellar sugar-sensing GRNs, and their optogenetic activation is sufficient to trigger proboscis extension[17]. Bract II connects to MN9 via two premotor neurons, Sink and Synch (S&S)[90] and Roundup[45]. S&S, predicted to be cholinergic, receives direct inputs from AN01B004, and outputs directly onto Roundup. Together, this circuit forms a sensory-motor arc connecting LgLG4 to MN9 through multiple positive feedforward loops.

Beyond proboscis extension, LgLG4 also engages downstream pathways that coordinate feeding with locomotor suppression and ingestion. Feeding and forward locomotion are mutually exclusive[17]. Flies feeding on a food patch suppress forward locomotion while still exhibiting micromovements around the patch[91,92]. Consistent with this, LgLG4 connects to Foxglove, a GABAergic neuron that suppresses forward walking[76], both directly via AN01B004 and indirectly via the S&S neuron (Figure 9B). In addition, another ascending neuron, AN05B106, connects LgLG4 GRNs to the pharyngeal pumping motor neuron MN11D (Figure S14B) and crop-entry motor neuron CEM (Figure S14C). We therefore propose that the LgLG4 pathway exemplifies how sensory input can be wired into circuits that simultaneously inhibit competing behaviors and promote feeding, thereby enforcing the behavioral switch from exploration to exploitation.

Descending control of motor actions by GRNs

Descending neurons (DNs) are information bottlenecks that connect the brain with the VNC. They integrate sensory information and behavioral states, and orchestrate various complex actions such as locomotion, courtship, and grooming[93]. As aforementioned, gustatory signals are important modulators of locomotion during foraging and sexual behavior. Furthermore, the detection of pathogenic bacteria triggers hygienic grooming via the activation of gustatory bristles on the anterior wing margin[94].

To understand how descending circuits integrate gustatory inputs, we performed a UMAP embedding of DN cell types based on their effective connectivity with different GRN types (Figure 9C). This analysis revealed five clusters, which we annotated by identifying functionally characterized DNs within them (Figure 9C). Strikingly, DNs known to control similar motor actions clustered together (Figure 9C): for example, most locomotion-related DNs[93] were part of a “locomotion cluster”. DNs that promote or suppress feeding are clustered in a “feeding cluster”. And the courtship-promoting DN aSP22[95] is found in a separate “courtship cluster”. One cluster, however, lacked functionally characterized members and therefore remains of unknown function. These results indicate that gustatory information is selectively routed into descending pathways that control distinct behavioral domains, providing a circuit framework through which taste can influence diverse motor programs.

As mentioned earlier, forward locomotion is suppressed during feeding. We therefore asked whether we can find evidence that appetitive proboscis GRNs contribute to this phenomenon. Our analysis revealed that LB3c, an appetitive lbGRN subtype, connects to two forward locomotion-promoting DNs, BDN2 and oDN1[96], through a circuit involving the interneurons Rattle, Fdg, and Foxglove (Figure 9D). Within this

circuit, Rattle and Fdg form a positive feedforward loop that activates Foxglove. Foxglove, in turn, inhibits both BDN2 and oDN1, thereby suppressing forward locomotion[96]. This identifies a direct neural pathway by which appetitive proboscis input could suppress locomotion, ensuring that the detection of food reliably promotes feeding over exploration

A particular descending neuron, DNg103, caught our attention because it shows very high effective connectivity scores with all attractive GRN types identified in this study (Figure 9E). DNg103 is predicted to be a GABAergic descending neuron that receives direct inputs from LgLG4, LgAG2, all LB3, and LB4 subtypes, with LgLG4 as its strongest GRN partner. Strikingly, DNg103 sends strong inhibitory feedback connections onto these attractive GRN types (Figure 9F). Such negative feedback loops are known to be sufficient to generate oscillatory dynamics, such as in transcriptional circadian oscillations[97]. Downstream, DNg103 connects to Bluebell, a neuron that induces stopping[96], via cholinergic AN01B004 and GABAergic GNG250 (Figure 9F). We therefore speculate that the reciprocal negative feedback between attractive GRNs and DNg103, could generate toggle switch/oscillatory activity in DNg103, which, in turn, would lead to stopping-walking sequences characteristic of feeding-related micromovements[91]. Such dynamics may provide a circuit mechanism for the micro-exploration of food patches that occurs once feeding is initiated.

Finally, we propose a novel role for ctpGRNs during courtship. Among all GRNs, ctpGRNs have the highest effective connectivity score with the courtship-promoting DN aSP22 (Figure S15A). Our analysis revealed that ctpGRN connects to aSP22 in 3 hops through multiple pathways, suggesting that *IR56d*-positive ctpGRN (Figure 3G) could contribute to the modulation of courtship (Figure S15B). As ctpGRNs are located between the pseudotrachea within the labellum, we speculate that they are likely to contribute to the courtship motor sequence triggered when males lick the genitalia of females.

Altogether, we used state-of-the-art connectomics to reconstruct and cell-type the entire gustatory connectome and feeding motor neurons of *Drosophila melanogaster* in maleCNS, MANC, and FAFB – FlyWire datasets (Figures 1 and 8). We combined morphological comparisons, synaptic connectivity and neurotransmitter predictions to identify unique GRN types and match them with receptor expression patterns allowing us to predict the tastants they detect (Figures 2-6 and 10A). UMAP embedding of downstream connectivity revealed novel attractive and aversive GRN types (Figures 7A and 10A). By analyzing effective connectivity between GRNs and effector neurons, we uncovered key high-order neurons and circuit motifs that might transform gustatory information into diverse outputs, such as neurosecretions, halting, proboscis extension, swallowing, ingestion, and courtship (Figures 8, 9, and 10B). Together, our work lays out a detailed gustatory sensorimotor connectome across multiple EM datasets, establishing a roadmap and hypothesis-generating platform to functionally dissect the neural circuit logic of conserved, state-dependent behavioral motor sequences such as feeding and mating.

Discussion

In his seminal work, “The Hungry Fly”[17], Vincent D. Dethier meticulously described the gustatory sensilla of the black blow fly, its feeding system, and its behavior and

noted: "*All of the intricate behavior patterns described here suggest that a study of the relation between sensory input and motor output would be a rewarding endeavor.*" Advances in molecular genetics and histological methods in *Drosophila melanogaster* allowed the field to pursue his vision, accelerated by the identification of taste receptors and followed by systematic physiological, anatomical, and behavioral studies that dissected the neural circuit mechanisms underlying feeding. Advances in EM connectomics in flies[11,12,27,28] now provide a unique opportunity to map the entire gustatory sensorimotor connectome with unprecedented detail. Work in fly larvae has already demonstrated the power of this approach, revealing how specific gustatory inputs are wired to motor and neuroendocrine outputs[77]. In adults, however, circuit knowledge has remained fragmentary. Previous studies have provided important insights into labellar bristle GRNs, including some morphological types, and their functional connection to the motor neuron MN9[45,98], but a comprehensive overview of gustatory circuits across body parts and motor outputs has been lacking.

Cell typing of GRNs

Here, we mapped the complete gustatory connectome of the fruit fly across three EM datasets: FAFB-FlyWire[12,27,28], MANC (male ventral nerve cord)[29,30], and maleCNS (entire male central nervous system) (Berg et al., 2025, in preparation). The maleCNS volume in particular enabled us to identify and annotate the full repertoire of gustatory receptor neurons in a single dataset (Figure 10). By combining neuroanatomical comparisons with synaptic connectivity and a consensus cell type atlas, we were able to finetune the annotation of GRN subtypes[99] (Berg et al., 2025, in preparation), allowing us to further refine the GRN types that recur across independent datasets. This cross-dataset reproducibility strongly supports our cell-typing rather than the different subclasses being due to individual variability. This approach revealed a remarkably diverse gustatory system, comprising four labellar bristle GRN types (lbGRNs; with a total of 15 subtypes), two taste peg GRN types (tpGRNs), 16 pharyngeal GRN types (phGRNs), nine directly ascending leg bristle GRN types (lgAGRNs), four wing bristle GRN types (wGRNs), and eight locally projecting leg bristle GRN types (lgLGRNs).

Notably, most pharyngeal GRNs are just a single pair of neurons, each projecting to distinct subsets of downstream circuits. This organization may provide a form of spatial discrimination within the pharynx, where different ingestion checkpoints are monitored by dedicated circuit units. A similar logic has been proposed for the expansion cell types in the dorsal root ganglia in vertebrates, where increased cellular diversity could enhance the spatial resolution of somatosensory inputs[100,101].

By matching the projection patterns of these GRNs to reporter lines, we could identify most of the previously described receptor-Gal4 cell types, adding further validity to our classification. In addition, we identified several GRN types that could not be matched to known driver lines, suggesting the existence of novel, yet unexplored GRN classes. Moreover, five aversive GRN classes that had been defined in classic electrophysiological and functional imaging studies reappear in our connectomic analysis, providing an independent line of support for our annotations[10,56]. In an accompanying study[47], we further functionally validated part of our cell typing by showing that taste peg GRNs differ in their function, and that only

one type (dtpGRNs) is necessary to regulate the length of yeast feeding bursts. This contrasts with the classic view that tpGRNs are one homogeneous group. Together, these lines of evidence support the robustness of our cell typing and reveal the strength of defining cell types using morphology, connectivity, and data across EM datasets. We propose that GRN types have distinct but overlapping roles in a wide range of biological functions, including foraging, feeding, sexual behavior, learning and memory, and neuromodulation (Figure 10).

Valence and Modularity

Our study further revealed how GRN diversity maps onto valence. UMAP embedding of GRNs based on downstream connectivity revealed that previously characterized attractive and aversive GRN types segregate into distinct clusters. These clusters also contain previously uncharacterized GRN types, suggesting that they likely encode the same valence as other GRNs in these clusters. Notably, both attractive and aversive clusters contained GRN types from different body parts, including legs, labellum, and pharynx, indicating that valence information from distributed gustatory sensilla on different sensory organs is integrated to generate unified perceptual decisions. At the same time, distinct sensorimotor pathways downstream of each GRN type would preserve compound-specific information to orchestrate the transformation to orchestrate the appropriate motor programs (Figures 10A and 10B). We propose that this modular organization, integrated valence coding combined with pathway-specific motor control, enables flexible adaptation of feeding behavior to changing external conditions and internal states.

Circuit motifs and functional validation

To move beyond direct synaptic partners, we used an effective connectivity metric that quantifies the relative strength of pathways linking GRNs to motor neurons across multiple synaptic hops[99]. This approach collapses the complexity of many possible routes into a normalized measure of influence, allowing us to identify the pathways most likely to be functionally relevant. Crucially, because we first identified and annotated the complete set of proboscis movement and ingestion motor neurons, we could bridge GRN inputs to specific motor outputs, rather than relying on other proxies. We identified key second-order, higher-order, and premotor neurons that receive inputs from a diverse set of aversive GRNs. We confirmed the functional validity of this approach in an accompanying study, where we showed that dtpGRNs are directly connected to pharyngeal pumping MNs, and that this pathway is important for regulating the length of feeding bursts on yeast by modulating ingestion efficiency[47].

Applying this analysis revealed two recurrent motifs by which attractive GRNs can control proboscis movements. First, a fast disinhibition pathway gates access to motor neurons controlling proboscis positioning and labellar spread. Such disinhibition might act as a thresholding mechanism, ensuring that the feeding motor program is only triggered when the stimulus is sufficiently strong. Second, a longer feedforward excitatory pathway recruits the same motor neurons with presumably slower dynamics, potentially coordinating their sustained activation during ongoing feeding (Figures 10A and 10B). We propose that this circuit architecture ensures avoiding the intake of harmful compounds by tonically inhibiting feeding at multiple circuit layers and potentially coordinating their sustained activation during ongoing

feeding via feedforward excitation. It will be crucial to test these hypotheses with functional experiments and activity recording approaches.

Interestingly, recent vertebrate work points to an analogous logic. A study in mice describes a multi-hop disinhibition motif spanning the amygdala–parabrachial–brainstem pathway that gates licking premotor neurons and thereby regulates lick-bout duration[102,103]. This suggests that recurrent disinhibition may represent a conserved circuit strategy for structuring ingestive bouts across species, from flies to mammals. More broadly, these findings highlight how motifs revealed by connectomics in the fly gustatory system can inform general principles of how sensory inputs are transformed into adaptive motor programs.

Specialization and flexibility

Our analysis also shows that most labellar bristle GRNs are more strongly connected to MNs controlling proboscis positioning, whereas most pharyngeal GRNs are predicted to control ingestion-related MNs. This general division reflects their anatomical position in the feeding sequence. Yet, exceptions such as LB2s connecting strongly to crop entry and PhG2s to proboscis positioning MNs highlight that not all GRNs follow this stereotypy. Such exceptions suggest functional flexibility, with select GRN types potentially allowing cross-talk between different subroutines of feeding.

Interestingly, effective connectivity patterns were largely conserved across sexes, with one notable exception: ctpGRNs seem to favor proboscis positioning over pharyngeal pumping MNs in the male, but the reverse is true in the female. Moreover, their connectivity to the courtship-promoting descending neuron aSP22 raises the possibility that ctpGRN might be involved in sexually dimorphic behaviors.

Sequential checkpoints and action control

Gustatory sensilla are exposed to chemical stimuli in a defined sequence during foraging and feeding: GRNs on the legs touch food first, allowing the fly to probe the food and decide if the proboscis should be extended. Labellar bristles then assess food quality, and if appropriate, labellar spread exposes taste pegs. Finally, coordinated pharyngeal muscle contractions pump the food into the cibarium, activating pharyngeal GRNs. Meanwhile, the fly suppresses forward locomotion to continue eating on the same food patch. Each GRN subclass thus acts as a checkpoint for transitions between subsequent motor actions based on their anatomical locations. These transitions are state-dependent, as demonstrated in both flies and mammals, where nutrient deprivation enhances initiation probabilities at multiple nodes of the feeding sequence[5].

Calculating the effective connectivity between leg GRNs and proboscis motor neurons, we showed that the attractive leg GRN type LgLG4 controls proboscis extension via an ascending neuron while suppressing forward locomotion through another interneuron. In turn, attractive labellar bristle GRNs can suppress locomotion by inhibiting forward locomotion DNs. In another study, we functionally characterized a sensorimotor circuit downstream of dtpGRNs that allows subsequent proboscis extensions by facilitating food swallowing[47]. Together, these circuits illustrate how

checkpoints are enforced and chained to ensure coherent action sequences, tuned by nutrient and mating states.

Decision bottlenecks in descending pathways

Taste is also important for controlling other behaviors, such as social behaviors and hygienic grooming. Descending neurons (DNs) act as bottlenecks where sensory information converges to be transformed into coordinated actions. UMAP embedding of DNs based on their effective connectivity with GRN types revealed clusters likely specialized for different actions. We identified a second-order inhibitory DN, DNg103, connected to attractive GRNs in a negative feedback loop. We speculate that this circuit generates oscillations, producing the characteristic intermittent stopping and moving “micromovements” in feeding flies via the stopping inducing DN, Bluebell. Comparable descending bottlenecks also exist in mammals, where gustatory signals in the brainstem converge onto reticulospinal and orofacial premotor neurons to implement licking and swallowing programs[104,105].

Anticipatory control of physiological state

Sensory perception is an important determinant of internal state modulation[106]. Here, we systematically explore how gustatory information in flies can reach neurosecretory cells via synaptic connections. Strikingly, only GRNs exposed to food upon ingestion or those tightly coupled to ingestion-related MNs are strongly connected to these endocrine outputs. This suggests a strategy to avoid undesired anticipatory changes in physiology based on noisy or irrelevant external cues, favoring signals linked to actual ingestion. Notably, putative sugar-sensing PhG1s connect to insulin-producing neurons, arguing that ingestion of caloric food can modify the satiety state in an anticipatory feedforward way. These mechanisms allow the fly to anticipatorily reprogram its physiology to prepare for the digestion of incoming food and switch from a catabolic to an anabolic state. This parallels cephalic-phase responses in mammals, where oropharyngeal inputs trigger endocrine release[107,108], though in flies, such modulation appears more tightly gated by ingestion checkpoints.

Conclusion

Our work provides a comprehensive and detailed gustatory sensorimotor connectome across multiple EM datasets in flies, establishing a blueprint to functionally dissect the neural circuit logic of conserved, state-dependent behavioral motor sequences underlying foraging, feeding, and mating. The detailed cell typing and effective connectivity analysis outlined here generate testable hypotheses about the logic of feeding control, from sensory checkpoints to descending bottlenecks, neuroendocrine coupling, and sexual dimorphisms. The powerful neurogenetic tools available in *Drosophila* make it possible to follow up on these predictions at cellular resolution. We are now in a unique position to unravel neural mechanisms underlying complex, adaptive sensorimotor transformations underlying foraging and feeding behaviors.

Acknowledgments

We thank the HHMI Janelia FlyEM project team and collaborators for pre-publication access to the male CNS dataset. We thank Lisa Marin, Marina Gkantia and other members of the Cambridge Connectomics Group based in the Department of Zoology for their input on cell annotation, especially in the VNC. We thank Ana Paula Elias for help with brain dissections and immunostainings. We thank Gabrielle Sterne and Attilio P. Ceretti for sharing MN annotations in FlyWire, Kathrin Eichler for help with the effective connectivity scripts, the Drosophila Connectomics Group, the Jefferis laboratory, and the whole Behaviour and Metabolism laboratory for many fruitful discussions, valuable feedback throughout the project, and comments on the manuscript. We thank the Champalimaud Fly and Rodent Platforms and the Champalimaud Advanced BioImaging and BioOptics Experimental Platform. Lines obtained from the Bloomington Drosophila Stock Center (NIH P40OD018537) were used in this study. I. T. was supported by a Marie Skłodowska-Curie postdoctoral fellowship (H2020-WF-01-2018-867459), R.B. was supported by a doctoral fellowship 2021.07285.BD from the Portuguese Foundation for Science and Technology (FCT). The project leading to these results has received funding from FCT (PTDC/MED-NEU/4001/2021), and the “la Caixa” Banking Foundation under the project codes HR17-00539 and HR23-00516 to C.R., Wellcome Trust Collaborative Award (220343/Z/20/Z) to G.S.X.E.J. with G. Rubin, G. Card, and S. Waddell, and an MRC Neuronex2 award (MC_EX_MR/T046279/1) and core support from the MRC (MC-U105188491) to G.S.X.E.J., A FENS Kavli Alumni Scientific Exchange Award From the Kavli Foundation and the Federation of European Neuroscience Societies to C.R. and G.S.X.E.J.. Research at the Centre for the Unknown is supported by the Champalimaud Foundation and by Portuguese national funds through FCT - Fundação para a Ciência e a Tecnologia - in the context of the project UIDB/04443/2020, the research infrastructure CONGENTO, co-financed by Lisboa Regional Operational Programme (Lisboa2020), under the PORTUGAL 2020 Partnership Agreement, through the European Regional Development Fund (ERDF) and FCT under the project LISBOA-01-0145-FEDER-022170, and the PPBI - LISBOA-01-0145-FEDER-022122.

Materials and Methods

Immunostaining and confocal imaging of brains and ventral nerve cords

Brains of 8-10 days old, fully fed, mated females expressing 20X-UAS-mCD8:GFP under the control of specific Split-Gal4 driver lines were used. Brains were dissected in 4 ◦C 1X PBS (10173433, Fisher Scientific, UK) after a quick passage through EtOH (4146052, Carlo Elba) and were then transferred to formaldehyde solution (4% paraformaldehyde, P6148, Sigma-Aldrich in 1X PBS + 10% Triton-X, X100, Sigma-Aldrich) and incubated for 20-30 min at room temperature. Samples were then washed three times in PBST (0.5% Triton-X in PBS) and then blocked with 10% normal goat serum (16210-064, Invitrogen) in PBST for 15-60 min at room temperature. Samples were then incubated in primary antibody solutions (Rabbit anti-GFP, TP401, Torrey Pines Biolabs at 1:6000 and Mouse anti-NC82, Developmental Studies Hybridoma Bank at 1:10 in 5% normal goat serum in PBST). Primary antibody incubations were performed for 3 days at 4 ◦C with rocking. They were then washed in PBST 2-3 times for 10-15 min at room temperature. The secondary antibodies were applied (Anti-mouse A594, A11032, Invitrogen at 1:500

and Anti-rabbit A488, A11008, Invitrogen at 1:500 in 5% normal goat serum in PBST) and brains were then incubated for 3 days at 4 ◦C with rocking. They were again washed in PBST 2-3 times for 10-15 min at room temperature. Samples were mounted in Vectashield Mounting Medium (H-1000, Vector Laboratories). For immunostaing, Janelia FlyLight protocol (IHC-MCFO, https://www.janelia.org/project-team/flylight/protocols) was used with a slight modification: the dehydration, clearing and DPX embedding steps were replaced with mounting in Vectashield Mounting Medium (VectorLabs, USA). Images were captured on an inverted Zeiss LSM 980 (Carl Zeiss Co., Oberkochen, Germany) using a Plan-ApoChromat 20x/0.8 air lens objective (Carl Zeiss Co., Oberkochen, Germany).

Confocal imaging of body parts

Wings, legs and heads of flies expressing 20X-UAS-mCD8:GFP and UAS-RedStinger (#BDSC: 8546) under *poxn*-GAL4[38], IR25a-GAL4 (#BDSC: 41728) or R57F03-GAL4 (#BDSC: 46386) were dissected using fine forceps (Dumond #5 forcepts, F.S.T., US) and mounted on a coverslip in either 1X PBS or 10S mineral oil (24627.188, VWR, France). Images were captured on an inverted Zeiss LSM 980 (Carl Zeiss Co., Oberkochen, Germany) using a Plan-ApoChromat 20x/ 0.8 N.A. air lens objective (Carl Zeiss Co., Oberkochen, Germany) or a Plan-ApoChromat 25X/0.8 N.A. multiimmersion lens.

GRN and MN identification, annotation and proofreading

As sensory neurons, the GRNs' axons of each subclass (labellar bristle, taste peg, pharyngeal, wing bristle and leg bristle GRNs) project to the CNS through specific nerves. Thus, in maleCNS, the GRNs of each subclass were identified and annotated by defining seed planes across their respective entering nerves. In FAFB – FlyWire and MANC, the GRNs were identified by previously defined annotations. To identify and annotate the MNs in maleCNS, we searched for morphological matches to previously annotated MNs in Flywire, in combination with defining seed planes through their exiting nerves.
The automated segmentation of each GRN and MN was individually evaluated to determine if proofreading was required. Any relevant splits or merges were identified and performed.

Connectomic partner analysis

The natverse package in R (R Develepment Core Team, version 4.1.0) was used to analyze the connectome dataset. The Dplyr package (https://github.com/tidyverse/dplyr) was used to facilitate data manipulation. To retrieve the synaptic-level connectome dataset and plot meshes, the fafbseg (for FAFB, FlyWire v783), malecns and manc packages were used via the coconatfly package (https://github.com/natverse/coconatfly?tab=readme-ov-file) (Schlegel et al Nature 2024). For synaptic connectivity predictions we used a cleft threshold = 50. Synaptic weight thresholds were indicated whenever applied. Graph representations of neuronal connectivity were plotted using Gephi (https://gephi.org/, version 0.10) to highlight relative connectivity of nodes. The neurons were treated as nodes and the synaptic connectivity between neurons were treated as directed edges scaled by the synaptic weights for each neuron pair. For the layout of the graphs, Built-in YiFan Hu Proportional method in Gephi was used. YiFan Hu's method is a time-efficient

method based on force-directed algorithm models that aim to minimize the energy in the system iteratively.

Matching neurons to the FAFB-FlyWire dataset

To cell type the GRNs and MNs in maleCNS based on their connectivity, we first cell typed their synaptic partners by matching them to their corresponding counterparts in FAFB – FlyWire[12,28,55], taking advantage of it being already a comprehensively typed connectome. We started by iteratively grouping the partners of our neurons of interest with similar connectivity and morphology. To, then, assign a FAFB – FlyWire type to each group, we compared the morphologies of the maleCNS neurons to their top 5 best matches in FAFB – FlyWire in a neuroglancer, which allows the simultaneous visualization of maleCNS meshes and transformed Flywire meshes to the maleCNS space. The top FAFB – FlyWire matches were found using pre-computed NBLAST scores resulting from comparisons between pairs of FAFB – FlyWire and maleCNS neuron skeletons that were registered on a common template space (Berg et al., 2025, in preparation). Finally, we selected the FAFB – FlyWire type with the closest morphology.

GRN and MN cell typing

To cell type the GRNs and MNs across connectomes, we used connectivity clustering based, respectively, on their outputs and inputs. As sensory neurons, each GRN establishes very few connections, and, so, except for pharyngeal GRNs, we used a threshold of 2 synapses for each GRN subclass. For MNs, we used the standard threshold of 5 synapses. To cluster neurons from either dataset or, when co-clustering from two different connectomes, we used cosine similarity scores that were computed using the coconatfly package (https://github.com/natverse/coconatfly). Briefly, this method computes the cosine similarity for pairs of connectivity vectors for neurons in the n-dimensional synaptic connectivity space. To assign types to defined connectivity clusters, we visualized and compared the morphologies of the neurons in each cluster to confirm a match. A complementary detailed inspection of top downstream partners and anatomical differences was used to, further, subtype the GRNs.

Effective connectivity algorithm

To make predictions on how a neuron's influence may impact another neuron across multiple synapses, we employed an effective connectivity algorithm based on serial matrix multiplication, adapted from a recent study[99]. To calculate effective connectivity scores between a given input and output neuron (or population) in the maleCNS or FAFB – FlyWire datasets, we used natverse, fafbseg and malecns R tools to first construct an all-by-all connectivity matrix representing the absolute number of synaptic connections between every pair of neurons in the dataset. This was then converted into a proportional matrix, where each neuron-to-neuron connection is expressed as the fraction of the postsynaptic neuron's total input synapses. Starting from a chosen set of 'input' neurons, we modeled the propagation of their influence through successive downstream layers by multiplying the corresponding rows of the proportional connectivity matrix by the full all-by-all proportional matrix. Each multiplication yielded an updated connectivity profile that represents how the input neuron's influence is redistributed through the outputs of its

direct partners, effectively extending the predicted impact one synaptic ‘hop’ further downstream. Iterating this procedure produced connectivity estimates across multiple layers of the network, up to a set number of ‘desired layers’. For each layer, we then extracted the effective connectivity values associated with a defined set of output neurons. To allow comparisons across inputs and layers, raw connection strengths were normalized by dividing each neuron’s score by the mean score of all neurons with non-zero values in that layer. This normalization ensured that effective connectivity scores reflected relative rather than absolute strengths, thereby highlighting disproportionately strong or weak pathways while controlling for global differences in connection density across layers.

Calculating significant paths

To construct the significant contributing neurons in a circuit between focal input and output neurons (or populations), we serially calculated effective connectivity scores from a focal input type to trace the strongest routes of influence across multiple synaptic layers. Starting from the downstream partners of the chosen input neurons, we first computed their effective connectivity score to the target population as described above. For each downstream layer, we then identified neurons whose normalized effective connectivity scores exceeded a threshold (80th quantile), thereby selecting candidates that most strongly underpin the transmission of influence from input to output. To further refine these candidates, we applied a pruning step in which each neuron was also evaluated for its effective connectivity from the original input population, ensuring that only those nodes maintaining a strong connection from the input population were retained. This set of candidates was then selected as a new ‘input’ with which to calculate effective connectivity to the output node in the next iteration, until the desired number of layers was reached. From this procedure, we are left with a list of influential neurons within the input to output circuit, from which we generated an all-by-all connectivity matrix, which was in turn used to generate circuit graphs using the Gephi graphing software.

Reachability analysis

To calculate reachability analysis between GRN and MN types, we ran successive iterations of effective connectivity calculations between each input and output pairing, while sequentially increasing the number of ‘desired layers’, used by the algorithm to model propagation of signal across multiple synaptic ‘hops’. The evolution of the effective connectivity scores between each cell-type connection was then plotted as a function of the increasing synaptic layer value.

References

1. Scott, K. Gustatory Processing in *Drosophila melanogaster*. *Annu. Rev. Entomol.* **63**, 15–30 (2018).
2. Moon, S. J., Lee, Y., Jiao, Y. & Montell, C. A *Drosophila* Gustatory Receptor Essential for Aversive Taste and Inhibiting Male-to-Male Courtship. *Curr. Biol.* **19**, 1623–1627 (2009).
3. Huetteroth, W. *et al.* Sweet Taste and Nutrient Value Subdivide Rewarding Dopaminergic Neurons in *Drosophila*. *Curr. Biol.* **25**, 751–758 (2015).
4. Chen, H.-L., Motevalli, D., Stern, U. & Yang, C.-H. A functional division of Drosophila sweet taste neurons that is value-based and task-specific. *Proc. Natl. Acad. Sci.* **119**, e2110158119 (2022).
5. Münch, D., Ezra-Nevo, G., Francisco, A. P., Tastekin, I. & Ribeiro, C. Nutrient homeostasis - translating internal states to behavior. *Curr. Opin. Neurobiol.* **60**, 67–75 (2020).
6. Amrein, H. & Thorne, N. Gustatory Perception and Behavior in *Drosophila melanogaster*. *Curr. Biol.* **15**, R673–R684 (2005).
7. Kwon, J. Y., Dahanukar, A., Weiss, L. A. & Carlson, J. R. A map of taste neuron projections in the Drosophila CNS. *J. Biosci.* **39**, 565–574 (2014).
8. Koh, T.-W. *et al.* The Drosophila IR20a Clade of Ionotropic Receptors Are Candidate Taste and Pheromone Receptors. *Neuron* **83**, 850–865 (2014).
9. Sánchez-Alcañiz, J. A. *et al.* An expression atlas of variant ionotropic glutamate receptors identifies a molecular basis of carbonation sensing. *Nat. Commun.* **9**, 4252 (2018).
10. Guillemin, J. *et al.* Taste cells expressing Ionotropic Receptor 94e reciprocally impact feeding and egg laying in Drosophila. *Cell Rep.* **43**, (2024).

11. Scheffer, L. K. *et al.* A connectome and analysis of the adult Drosophila central brain. *eLife* **9**, e57443 (2020).
12. Dorkenwald, S. *et al.* Neuronal wiring diagram of an adult brain. *Nature* **634**, 124–138 (2024).
13. Baik, L. S. & Carlson, J. R. The mosquito taste system and disease control. *Proc. Natl. Acad. Sci.* **117**, 32848–32856 (2020).
14. Baik, L. S. *et al.* Mosquito taste responses to human and floral cues guide biting and feeding. *Nature* **635**, 639–646 (2024).
15. Muth, F., Francis, J. S. & Leonard, A. S. Bees use the taste of pollen to determine which flowers to visit. *Biol. Lett.* **12**, 20160356 (2016).
16. Dweck, H. K., Talross, G. J., Wang, W. & Carlson, J. R. Evolutionary shifts in taste coding in the fruit pest Drosophila suzukii. *eLife* **10**, e64317 (2021).
17. Dethier, V. G. *The Hungry Fly: A Physiological Study of the Behavior Associated with Feeding*. 489 (Harvard U Press, Oxford, England, 1976).
18. Stocker, R. F. The organization of the chemosensory system in Drosophila melanogaster: a review. *Cell Tissue Res.* **275**, 3–26 (1994).
19. Rajashekhar, K. P. & Singh, R. N. Organization of motor neurons innervating the proboscis musculature in *Drosophila melanogaster* meigen (diptera : Drosophilidae). *Int. J. Insect Morphol. Embryol.* **23**, 225–242 (1994).
20. Gordon, M. D. & Scott, K. Motor Control in a *Drosophila* Taste Circuit. *Neuron* **61**, 373–384 (2009).
21. Flood, T. F. *et al.* A single pair of interneurons commands the Drosophila feeding motor program. *Nature* **499**, 83–87 (2013).
22. Schwarz, O. *et al.* Motor control of Drosophila feeding behavior. *eLife* **6**, e19892 (2017).

23. McKellar, C. E., Siwanowicz, I., Dickson, B. J. & Simpson, J. H. Controlling motor neurons of every muscle for fly proboscis reaching. *eLife* **9**, e54978 (2020).
24. Nern, A. *et al.* Connectome-driven neural inventory of a complete visual system. *Nature* **641**, 1225–1237 (2025).
25. Bates, A. S. *et al.* Complete Connectomic Reconstruction of Olfactory Projection Neurons in the Fly Brain. *Curr. Biol. CB* **30**, 3183-3199.e6 (2020).
26. Eichler, K. *et al.* Somatotopic organization among parallel sensory pathways that promote a grooming sequence in Drosophila. *eLife* **12**, (2024).
27. Zheng, Z. *et al.* A Complete Electron Microscopy Volume of the Brain of Adult *Drosophila melanogaster*. *Cell* **174**, 730-743.e22 (2018).
28. Schlegel, P. *et al.* Whole-brain annotation and multi-connectome cell typing of Drosophila. *Nature* **634**, 139–152 (2024).
29. Takemura, S. *et al.* A Connectome of the Male Drosophila Ventral Nerve Cord. *eLife* **13**, (2024).
30. Marin, E. C. *et al.* Systematic annotation of a complete adult male Drosophila nerve cord connectome reveals principles of functional organisation. *eLife* **13**, (2024).
31. Cheong, H. S. *et al.* Transforming descending input into motor output: An analysis of the Drosophila Male Adult Nerve Cord connectome. *eLife* **13**, (2025).
32. Engert, S., Sterne, G. R., Bock, D. D. & Scott, K. Drosophila gustatory projections are segregated by taste modality and connectivity. *eLife* **11**, e78110 (2022).
33. Nayak, S. V. & Singh, R. N. Sensilla on the tarsal segments and mouthparts of adult *Drosophila melanogaster* meigen (Diptera : Drosophilidae). *Int. J. Insect Morphol. Embryol.* **12**, 273–291 (1983).

34. Shanbhag, S., Park, S.-K., Pikielny, C. & Steinbrecht, R. Gustatory organs of Drosophila melanogaster: fine structure and expression of the putative odorant-binding protein PBPRP2. *Cell Tissue Res.* **304**, 423–437 (2001).
35. Palka, J., Lawrence, P. A. & Hart, H. S. Neural projection patterns from homeotic tissue of *Drosophila* studied in *bithorax* mutants and mosaics. *Dev. Biol.* **69**, 549–575 (1979).
36. Palka, J. Neuronal specificity and its development in the Drosophila wing disc and its derivatives. *J. Neurobiol.* **24**, 788–802 (1993).
37. Chen, Y.-C. D. & Dahanukar, A. Molecular and Cellular Organization of Taste Neurons in Adult *Drosophila* Pharynx. *Cell Rep.* **21**, 2978–2991 (2017).
38. Boll, W. & Noll, M. The Drosophila Pox neuro gene: control of male courtship behavior and fertility as revealed by a complete dissection of all enhancers. *Dev. Camb. Engl.* **129**, 5667–5681 (2002).
39. Thoma, V. *et al.* Functional dissociation in sweet taste receptor neurons between and within taste organs of Drosophila. *Nat. Commun.* **7**, 10678 (2016).
40. Robertson, H. M. Chemical stimuli eliciting courtship by males inDrosophila melanogaster. *Experientia* **39**, 333–335 (1983).
41. Lu, B., LaMora, A., Sun, Y., Welsh, M. J. & Ben-Shahar, Y. ppk23-Dependent Chemosensory Functions Contribute to Courtship Behavior in Drosophila melanogaster. *PLOS Genet.* **8**, e1002587 (2012).
42. Thistle, R., Cameron, P., Ghorayshi, A., Dennison, L. & Scott, K. Contact Chemoreceptors Mediate Male-Male Repulsion and Male-Female Attraction during Drosophila Courtship. *Cell* **149**, 1140–1151 (2012).

43. Raad, H., Ferveur, J.-F., Ledger, N., Capovilla, M. & Robichon, A. Functional Gustatory Role of Chemoreceptors in *Drosophila* Wings. *Cell Rep.* **15**, 1442–1454 (2016).
44. He, Z., Luo, Y., Shang, X., Sun, J. S. & Carlson, J. R. Chemosensory sensilla of the Drosophila wing express a candidate ionotropic pheromone receptor. *PLOS Biol.* **17**, e2006619 (2019).
45. Shiu, P. K., Sterne, G. R., Engert, S., Dickson, B. J. & Scott, K. Taste quality and hunger interactions in a feeding sensorimotor circuit. *eLife* **11**, e79887 (2022).
46. Steck, K. *et al.* Internal amino acid state modulates yeast taste neurons to support protein homeostasis in Drosophila. *eLife* **7**, e31625 (2018).
47. Tastekin, I. *et al.* Connectomics Reveals a Feed-Forward Swallowing Circuit Driving Protein Appetite. (2025).
48. Naresh Singh, R. & Nayak, S. V. Fine structure and primary sensory projections of sensilla on the maxillary palp of *Drosophila melanogaster* Meigen (Diptera : Drosophilidae). *Int. J. Insect Morphol. Embryol.* **14**, 291–306 (1985).
49. LeDue, E. E., Chen, Y.-C., Jung, A. Y., Dahanukar, A. & Gordon, M. D. Pharyngeal sense organs drive robust sugar consumption in Drosophila. *Nat. Commun.* **6**, 6667 (2015).
50. Sang, J. *et al.* A single pair of pharyngeal neurons functions as a commander to reject high salt in Drosophila melanogaster. *eLife* **12**, (2024).
51. Miyazaki, T. & Ito, K. Neural architecture of the primary gustatory center of Drosophila melanogaster visualized with GAL4 and LexA enhancer-trap systems. *J. Comp. Neurol.* **518**, 4147–4181 (2010).

52. Murphey, R. K., Possidente, D., Pollack, G. & Merritt, D. J. Modality-specific axonal projections in the CNS of the flies Phormia and Drosophila. *J. Comp. Neurol.* **290**, 185–200 (1989).
53. Possidente, D. R. & Murphey, R. K. Genetic control of sexually dimorphic axon morphology in *Drosophila* sensory neurons. *Dev. Biol.* **132**, 448–457 (1989).
54. Singh, R. N. Neurobiology of the gustatory systems of Drosophila and some terrestrial insects. *Microsc. Res. Tech.* **39**, 547–563 (1997).
55. Eckstein, N. *et al.* Neurotransmitter classification from electron microscopy images at synaptic sites in *Drosophila melanogaster*. *Cell* **187**, 2574-2594.e23 (2024).
56. Weiss, L. A., Dahanukar, A., Kwon, J. Y., Banerjee, D. & Carlson, J. R. The Molecular and Cellular Basis of Bitter Taste in *Drosophila*. *Neuron* **69**, 258–272 (2011).
57. Fujii, S. *et al.* Drosophila Sugar Receptors in Sweet Taste Perception, Olfaction and Internal Nutrient Sensing. *Curr. Biol. CB* **25**, 621–627 (2015).
58. Jaeger, A. H. *et al.* A complex peripheral code for salt taste in Drosophila. *eLife* **7**, e37167 (2018).
59. McDowell, S. A. T., Stanley, M. & Gordon, M. D. A molecular mechanism for high salt taste in *Drosophila*. *Curr. Biol.* **32**, 3070-3081.e5 (2022).
60. Starostina, E. *et al.* A Drosophila DEG/ENaC Subunit Functions Specifically in Gustatory Neurons Required for Male Courtship Behavior. *J. Neurosci.* **32**, 4665–4674 (2012).
61. Rytz, R., Croset, V. & Benton, R. Ionotropic Receptors (IRs): Chemosensory ionotropic glutamate receptors in *Drosophila* and beyond. *Insect Biochem. Mol. Biol.* **43**, 888–897 (2013).

62. Inoshita, T. & Tanimura, T. Cellular identification of water gustatory receptor neurons and their central projection pattern in Drosophila. *Proc. Natl. Acad. Sci.* **103**, 1094–1099 (2006).

63. Cameron, P., Hiroi, M., Ngai, J. & Scott, K. The molecular basis for water taste in Drosophila. *Nature* **465**, 91–95 (2010).

64. Dweck, H. K. M., Talross, G. J. S., Luo, Y., Ebrahim, S. A. M. & Carlson, J. R. Ir56b is an atypical ionotropic receptor that underlies appetitive salt response in *Drosophila*. *Curr. Biol.* **32**, 1776-1787.e4 (2022).

65. Wisotsky, Z., Medina, A., Freeman, E. & Dahanukar, A. Evolutionary differences in food preference rely on Gr64e, a receptor for glycerol. *Nat. Neurosci.* **14**, 1534–1541 (2011).

66. Brown, E. B. *et al.* Ir56d-dependent fatty acid responses in Drosophila uncover taste discrimination between different classes of fatty acids. *eLife* **10**, e67878 (2021).

67. Luo, Y., Talross, G. J. S. & Carlson, J. R. Function and evolution of Ir52 receptors in mate detection in Drosophila. *Curr. Biol.* **34**, 5395-5408.e6 (2024).

68. Taisz, I. *et al.* Generating parallel representations of position and identity in the olfactory system. *Cell* **186**, 2556-2573.e22 (2023).

69. Ling, F., Dahanukar, A., Weiss, L. A., Kwon, J. Y. & Carlson, J. R. The Molecular and Cellular Basis of Taste Coding in the Legs of Drosophila. *J. Neurosci.* **34**, 7148–7164 (2014).

70. Kim, H., Kirkhart, C. & Scott, K. Long-range projection neurons in the taste circuit of Drosophila. *eLife* **6**, e23386 (2017).

71. Fan, P. *et al.* Genetic and Neural Mechanisms that Inhibit *Drosophila* from Mating with Other Species. *Cell* **154**, 89–102 (2013).

72. Kallman, B. R., Kim, H. & Scott, K. Excitation and inhibition onto central courtship neurons biases Drosophila mate choice. *eLife* **4**, e11188 (2015).

73. Dahanukar, A., Lei, Y.-T., Kwon, J. Y. & Carlson, J. R. Two *Gr* Genes Underlie Sugar Reception in *Drosophila*. *Neuron* **56**, 503–516 (2007).

74. Kohatsu, S., Tanabe, N., Yamamoto, D. & Isono, K. Which Sugar to Take and How Much to Take? Two Distinct Decisions Mediated by Separate Sensory Channels. *Front. Mol. Neurosci.* **15**, (2022).

75. Chen, Y.-C. D., Park, S. J., Joseph, R. M., Ja, W. W. & Dahanukar, A. A. Combinatorial Pharyngeal Taste Coding for Feeding Avoidance in Adult Drosophila. *Cell Rep.* **29**, 961-973.e4 (2019).

76. Bidaye, S. S. *et al.* Two Brain Pathways Initiate Distinct Forward Walking Programs in *Drosophila*. *Neuron* **108**, 469-485.e8 (2020).

77. Miroschnikow, A., Schlegel, P. & Pankratz, M. J. Making Feeding Decisions in the *Drosophila* Nervous System. *Curr. Biol.* **30**, R831–R840 (2020).

78. Münch, D., Goldschmidt, D. & Ribeiro, C. The neuronal logic of how internal states control food choice. *Nature* **607**, 747–755 (2022).

79. Cui, X., Meiselman, M. R., Thornton, S. N. & Yapici, N. A gut-brain-gut interoceptive circuit loop gates sugar ingestion in Drosophila. 2024.09.02.610892 Preprint at https://doi.org/10.1101/2024.09.02.610892 (2024).

80. Manzo, A., Silies, M., Gohl, D. M. & Scott, K. Motor neurons controlling fluid ingestion in Drosophila. *Proc. Natl. Acad. Sci. U. S. A.* **109**, 6307–6312 (2012).

81. Itskov, P. M. *et al.* Automated monitoring and quantitative analysis of feeding behaviour in Drosophila. *Nat. Commun.* **5**, 4560 (2014).

82. Chen, Y., Lin, Y.-C., Kuo, T.-W. & Knight, Z. A. Sensory Detection of Food Rapidly Modulates Arcuate Feeding Circuits. *Cell* **160**, 829–841 (2015).

83. Garfield, A. S. *et al.* Dynamic GABAergic afferent modulation of AgRP neurons. *Nat. Neurosci.* **19**, 1628–1635 (2016).

84. Ly, T. *et al.* Sequential appetite suppression by oral and visceral feedback to the brainstem. *Nature* **624**, 130–137 (2023).

85. Brandt, C. *et al.* Food Perception Primes Hepatic ER Homeostasis via Melanocortin-Dependent Control of mTOR Activation. *Cell* **175**, 1321-1335.e20 (2018).

86. Tsuneki, H. *et al.* Food odor perception promotes systemic lipid utilization. *Nat. Metab.* **4**, 1514–1531 (2022).

87. Burke, L. K. *et al.* mTORC1 in AGRP neurons integrates exteroceptive and interoceptive food-related cues in the modulation of adaptive energy expenditure in mice. *eLife* **6**, e22848 (2017).

88. Zandawala, M. & Gera, J. Leptin- and cytokine-like unpaired signaling in Drosophila. *Mol. Cell. Endocrinol.* **584**, 112165 (2024).

89. Chen, Y. & Knight, Z. A. Making sense of the sensory regulation of hunger neurons. *BioEssays* **38**, 316–324 (2016).

90. Sterne, G. R., Otsuna, H., Dickson, B. J. & Scott, K. Classification and genetic targeting of cell types in the primary taste and premotor center of the adult Drosophila brain. *eLife* **10**, e71679 (2021).

91. Corrales-Carvajal, V. M., Faisal, A. A. & Ribeiro, C. Internal states drive nutrient homeostasis by modulating exploration-exploitation trade-off. *eLife* **5**, e19920 (2016).

92. Goldschmidt, D. *et al.* A neuronal substrate for translating nutrient state and resource density estimations into foraging decisions. 2023.07.19.549514 Preprint at https://doi.org/10.1101/2023.07.19.549514 (2023).

93. Simpson, J. H. Descending control of motor sequences in Drosophila. *Curr. Opin. Neurobiol.* **84**, 102822 (2024).

94. Yanagawa, A., Guigue, A. M. A. & Marion-Poll, F. Hygienic grooming is induced by contact chemicals in Drosophila melanogaster. *Front. Behav. Neurosci.* **8**, (2014).

95. McKellar, C. E. *et al.* Threshold-Based Ordering of Sequential Actions during Drosophila Courtship. *Curr. Biol. CB* **29**, 426-434.e6 (2019).

96. Sapkal, N. *et al.* Neural circuit mechanisms underlying context-specific halting in Drosophila. *Nature* **634**, 191–200 (2024).

97. Smolen, P., Baxter, D. A. & Byrne, J. H. Modeling Circadian Oscillations with Interlocking Positive and Negative Feedback Loops. *J. Neurosci.* **21**, 6644–6656 (2001).

98. Shiu, P. K. *et al.* A Drosophila computational brain model reveals sensorimotor processing. *Nature* **634**, 210–219 (2024).

99. Stürner, T. *et al.* Comparative connectomics of Drosophila descending and ascending neurons. *Nature* **643**, 158–172 (2025).

100. Sharma, N. *et al.* The emergence of transcriptional identity in somatosensory neurons. *Nature* **577**, 392–398 (2020).

101. Ran, C., Boettcher, J. C., Kaye, J. A., Gallori, C. E. & Liberles, S. D. A brainstem map for visceral sensations. *Nature* **609**, 320–326 (2022).

102. Nakamura, K. & Nakamura, Y. Hunger and Satiety Signaling: Modeling Two Hypothalamomedullary Pathways for Energy Homeostasis. *BioEssays News Rev. Mol. Cell. Dev. Biol.* **40**, e1700252 (2018).

103. Lafferty, D. S. *et al.* An amygdalopontine pathway promotes motor programs of ingestion. 2025.06.05.657686 Preprint at https://doi.org/10.1101/2025.06.05.657686 (2025).

104. Grill, H. J. & Norgren, R. The taste reactivity test. II. Mimetic responses to gustatory stimuli in chronic thalamic and chronic decerebrate rats. *Brain Res.* **143**, 281–297 (1978).

105. Travers, J. B. Motor Control of Feeding and Drinking. in *Encyclopedia of Neuroscience* (ed. Squire, L. R.) 1001–1007 (Academic Press, Oxford, 2009). doi:10.1016/B978-008045046-9.00449-6.

106. Yao, Z. & Scott, K. Serotonergic neurons translate taste detection into internal nutrient regulation. *Neuron* **110**, 1036-1050.e7 (2022).

107. Just, T., Pau, H. W., Engel, U. & Hummel, T. Cephalic phase insulin release in healthy humans after taste stimulation? *Appetite* **51**, 622–627 (2008).

108. Power, M. L. & Schulkin, J. Anticipatory physiological regulation in feeding biology: Cephalic phase responses. *Appetite* **50**, 194–206 (2008).

Figures

Figure 1

A Taste sensilla at the light level

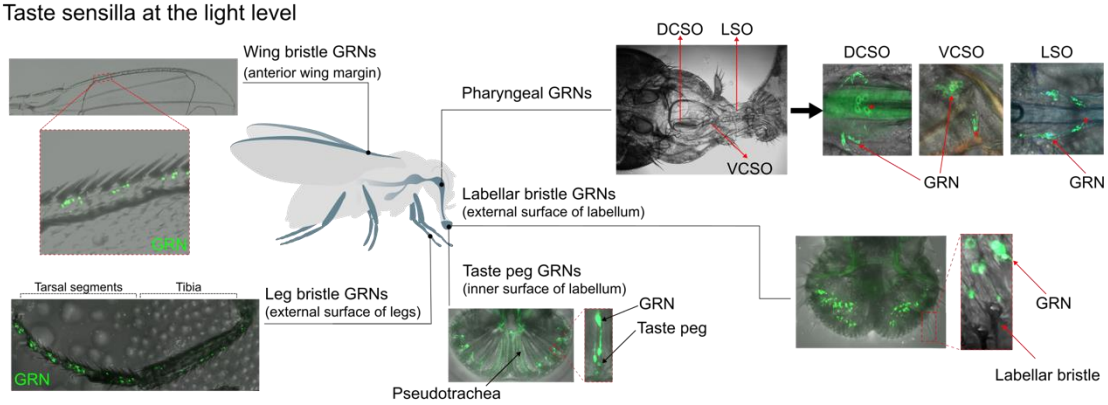

B GRN projections in the CNS at the light level

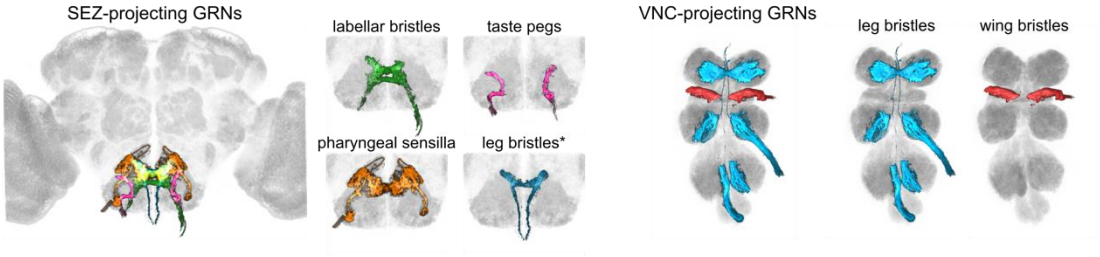

C MaleCNS (mc) GRN projections

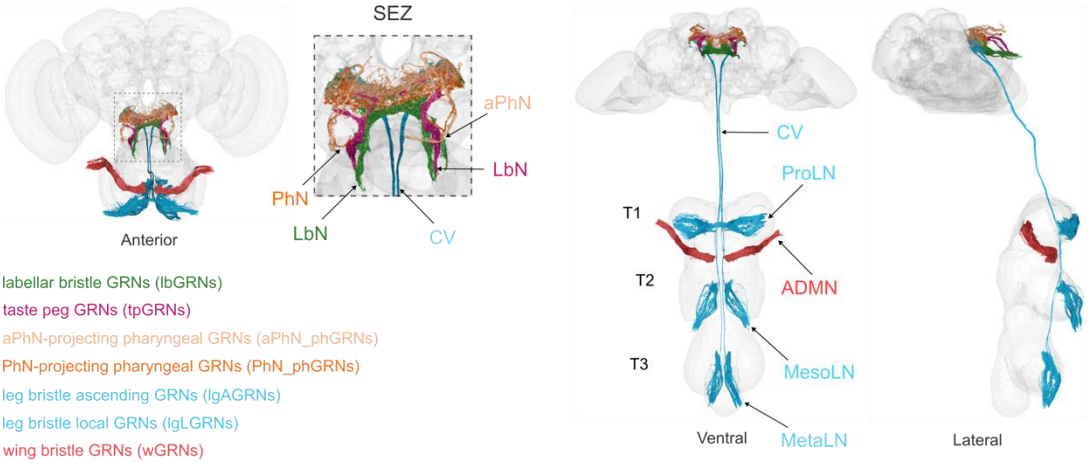

D MANC (mv) GRN projections

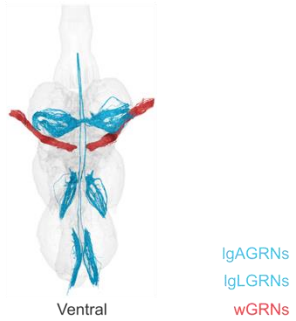

E Flywire (fw) GRN projections

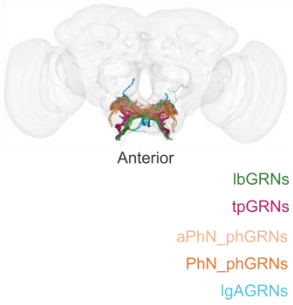

F GRNs: Counts

	mc		fw		mv		SD
	R	L	R	L	R	L	
lbGRNs	90	90	105	108	-	-	No
tpGRNs	30	30	37	37	-	-	Yes
aPhN_phGRNs	18	18	19	18	-	-	No
PhN_phGRNs	6	6	7	6	-	-	No
lgAGRNs	39	40	37	37	39	39	No
lgLGRNs	348	343	-	-	335	315	-
wGRNs	192	193	-	-	198	194	-

Figure 2

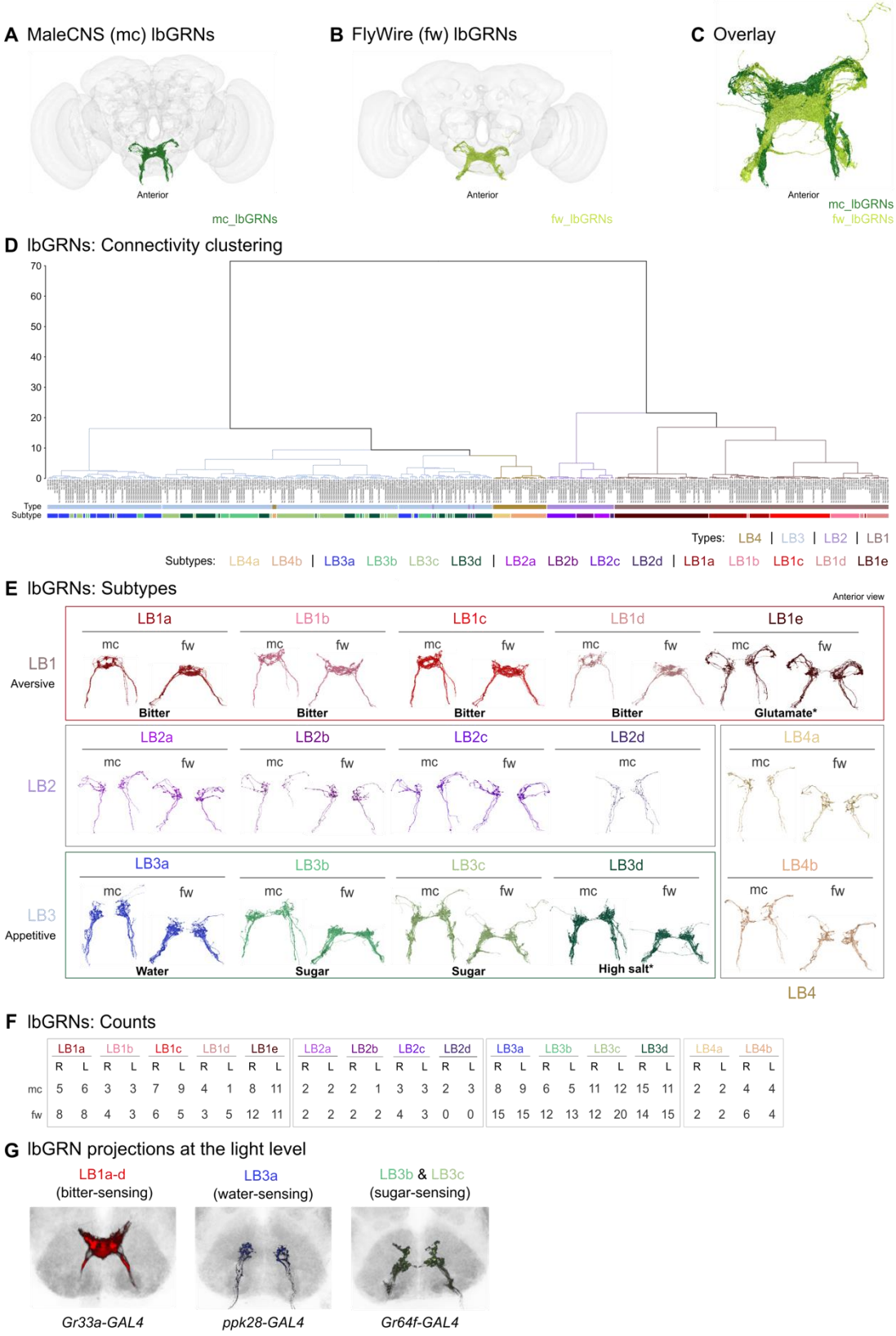

F lbGRNs: Counts

	LB1a		LB1b		LB1c		LB1d		LB1e		LB2a		LB2b		LB2c		LB2d		LB3a		LB3b		LB3c		LB3d		LB4a		LB4b	
	R	L	R	L	R	L	R	L	R	L	R	L	R	L	R	L	R	L	R	L	R	L	R	L	R	L	R	L	R	L
mc	5	6	3	3	7	9	4	1	8	11	2	2	2	1	3	3	2	3	8	9	6	5	11	12	15	11	2	2	4	4
fw	8	8	4	3	6	5	3	5	12	11	2	2	2	2	4	3	0	0	15	15	12	13	12	20	14	15	2	2	6	4

G lbGRN projections at the light level

Figure 3

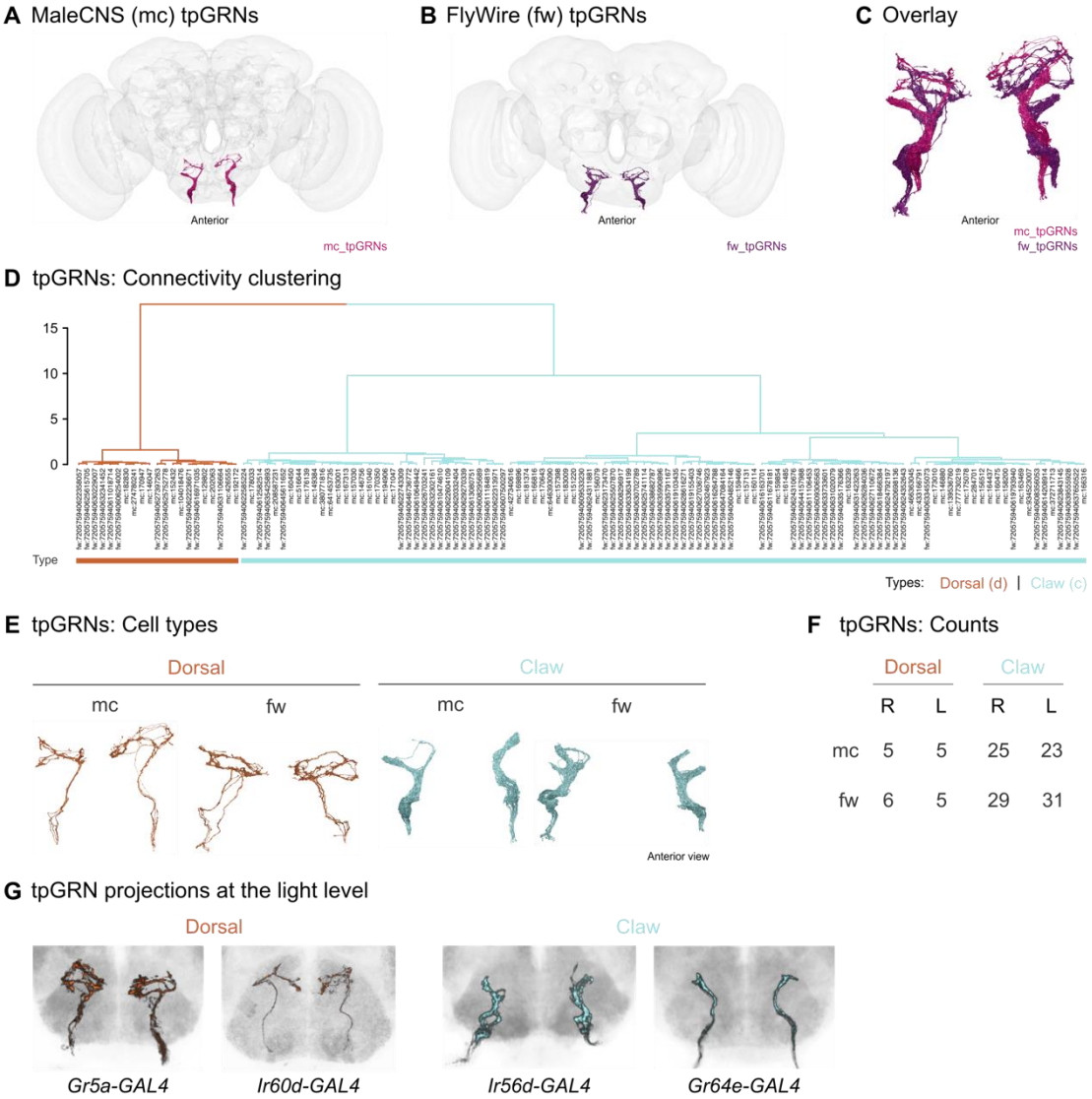

	Dorsal		Claw	
	R	L	R	L
mc	5	5	25	23
fw	6	5	29	31

Figure 4

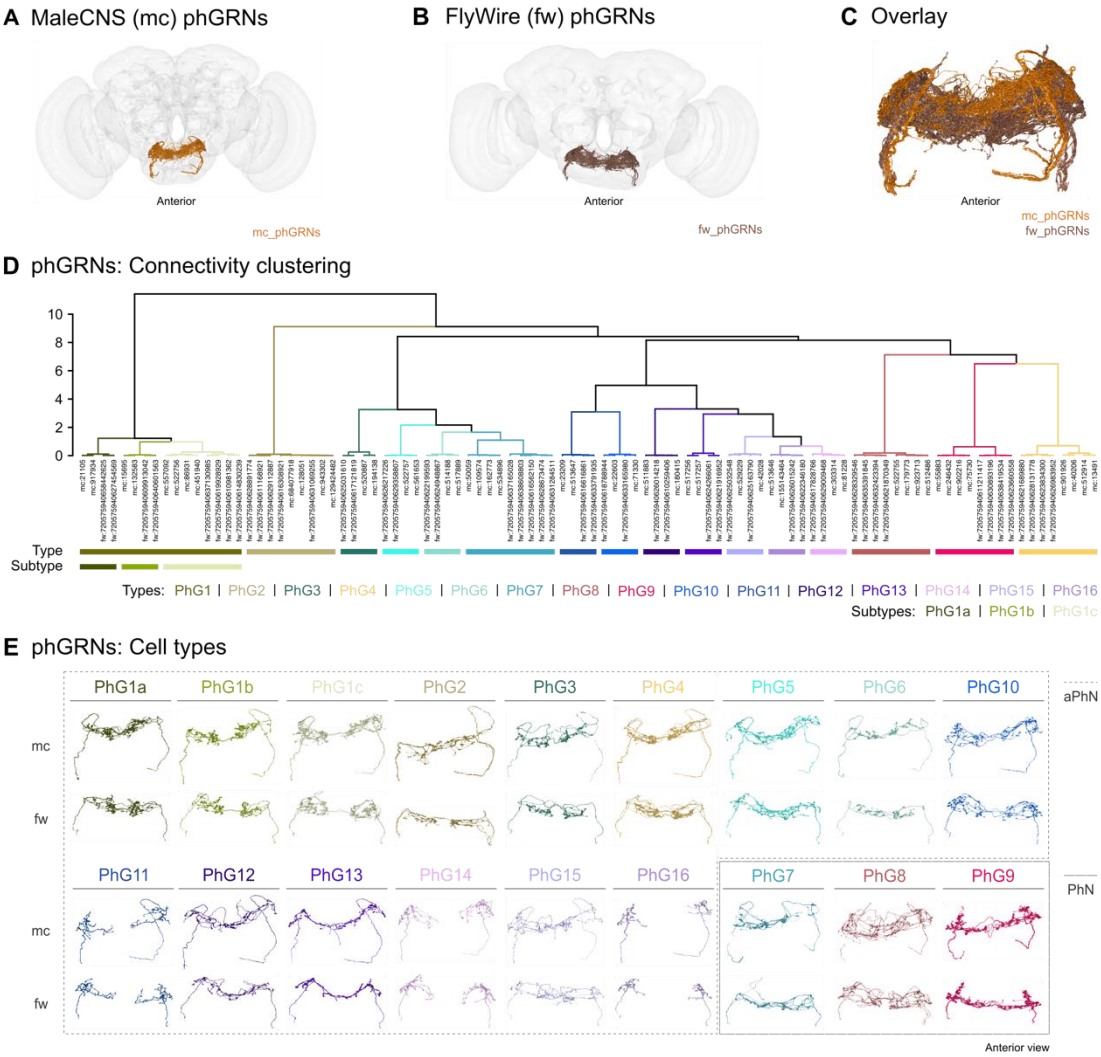

F phGRNs: Counts

	PhG1a		PhG1b		PhG1c		PhG2		PhG3		PhG4		PhG5		PhG6		PhG7		PhG8		PhG9		PhG10		PhG11		PhG12		PhG13		PhG14		PhG15		PhG16	
	R	L	R	L	R	L	R	L	R	L	R	L	R	L	R	L	R	L	R	L	R	L	R	L	R	L	R	L	R	L	R	L	R	L	R	L
mc	1	1	1	1	2	2	2	2	1	1	2	2	1	1	1	1	2	2	2	2	2	2	1	1	1	1	1	1	1	1	1	1	1	1	1	1
fw	1	1	1	1	2	2	3	2	1	1	2	2	1	1	1	1	3	2	2	2	2	2	1	1	1	1	1	1	1	1	1	1	1	1	1	1

G phGRN projections at the light level

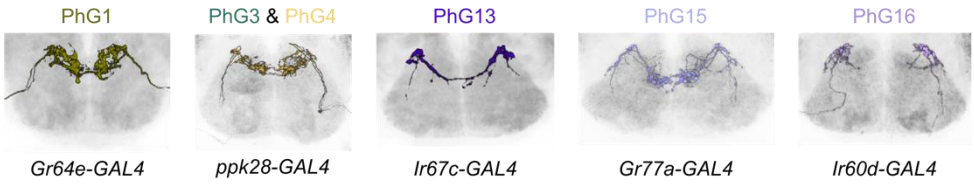

Figure 5

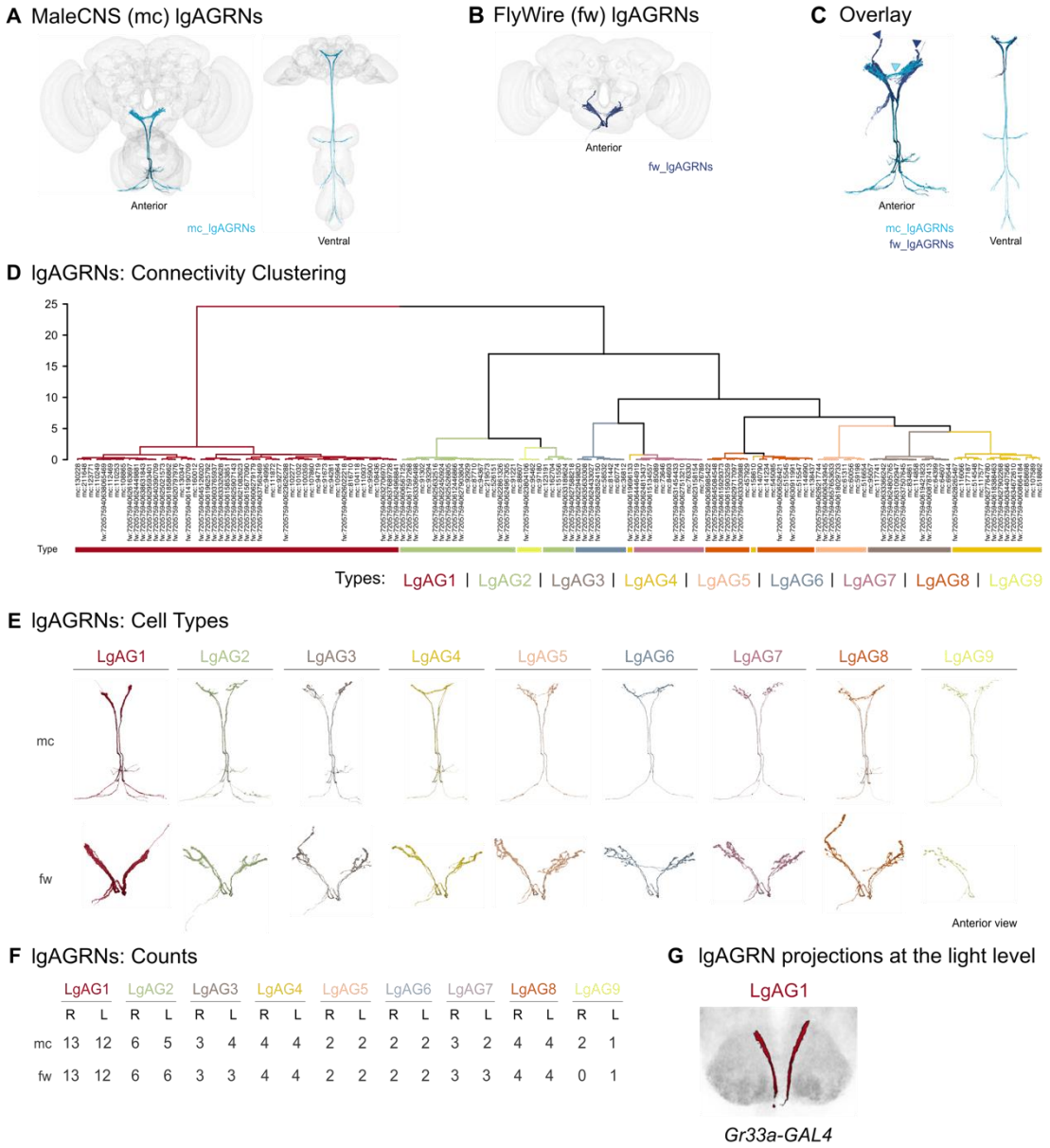

F lgAGRNs: Counts

	LgAG1		LgAG2		LgAG3		LgAG4		LgAG5		LgAG6		LgAG7		LgAG8		LgAG9	
	R	L	R	L	R	L	R	L	R	L	R	L	R	L	R	L	R	L
mc	13	12	6	5	3	4	4	4	2	2	2	2	3	2	4	4	2	1
fw	13	12	6	6	3	3	4	4	2	2	2	2	3	3	4	4	0	1

G lgAGRN projections at the light level

LgAG1

Gr33a-GAL4

Figure 6

A MaleCNS (mc) w- and lgLGRNs

B MANC (mv) w- and lgLGRNs

C wGRNs: Connectivity clustering

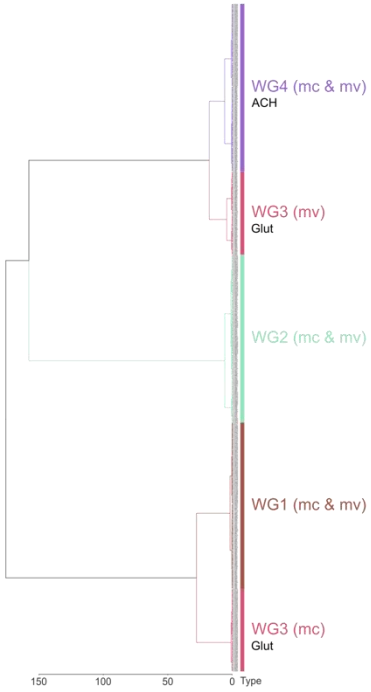

D wGRNs: Cell types

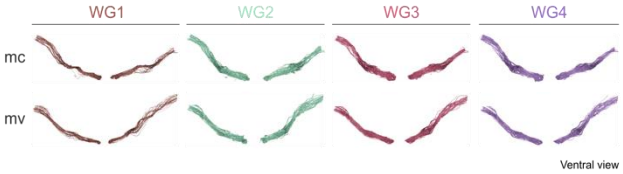

E wGRNs: Counts

	WG1		WG2		WG3		WG4	
	R	L	R	L	R	L	R	L
mc	48	48	48	49	48	48	48	48
mv	50	48	49	49	49	48	50	49

F wGRNs: All types

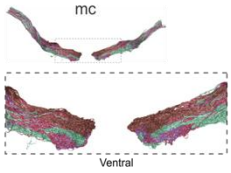

G Foreleg LGRNs: Connectivity clustering

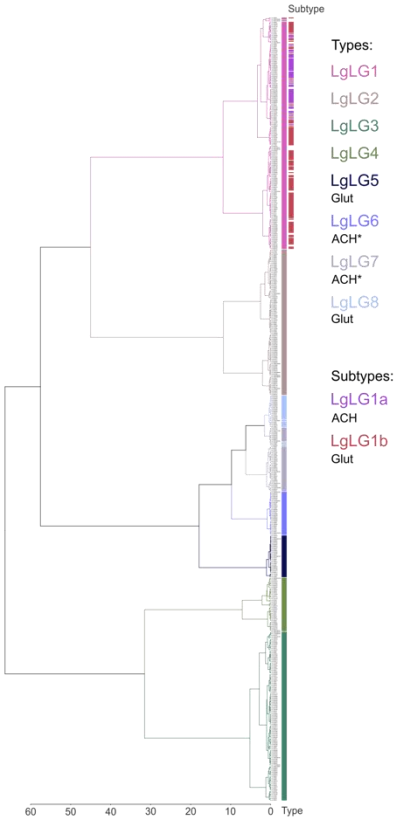

H lgLGRNs: Cell types

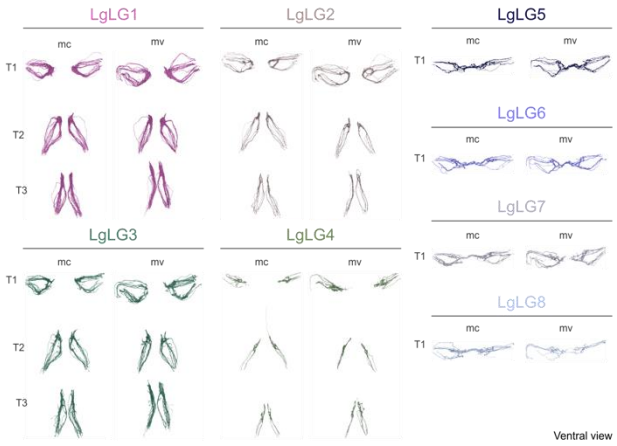

J Foreleg LGRNs: Counts

	LgLG1 (a/b)		LgLG2		LgLG3		LgLG4		LgLG5		LgLG6		LgLG7		LgLG8	
	R	L	R	L	R	L	R	L	R	L	R	L	R	L	R	L
mc	42 (17/16)	41 (17/20)	22	24	33	29	7	8	7	6	7	8	10	12	8	6
mv	35 (4/31)	40 (5/35)	29	26	23	30	14	9	8	8	7	8	11	10	5	4

Figure 7

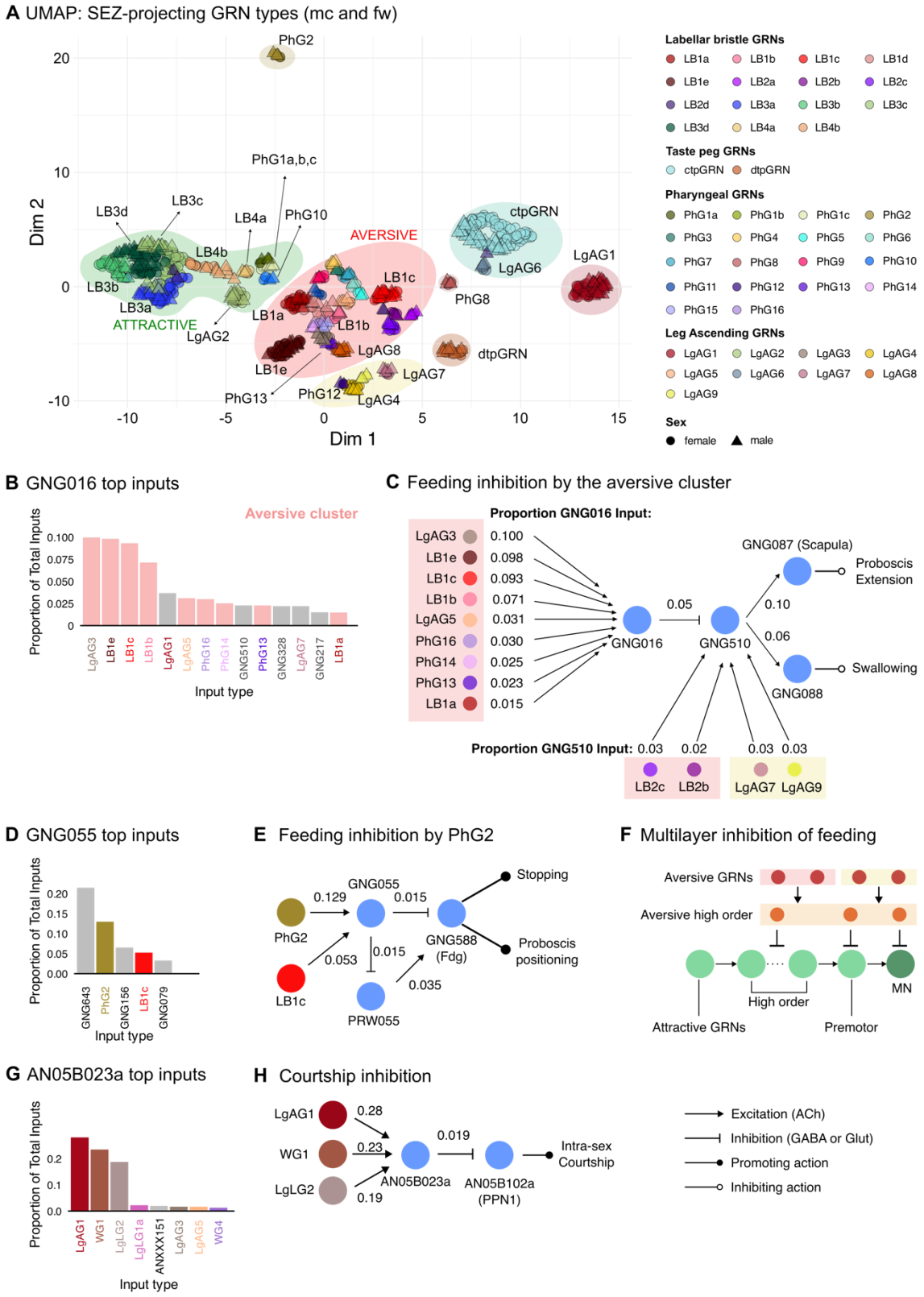
A UMAP: SEZ-projecting GRN types (mc and fw)
Dim 1
Dim 2
PhG2
PhG1a,b,c
LB3d
LB3c
LB4a
PhG10
LB4b
LB3b
LB3a
ATTRACTIVE
LgAG2
AVERSIVE
LB1c
LB1a
LB1b
LB1e
LgAG8
LgAG7
LgAG4
PhG13
PhG12
ctpGRN
LgAG6
LgAG1
PhG8
dtpGRN
Labellar bristle GRNs
Taste peg GRNs
Pharyngeal GRNs
Leg Ascending GRNs
Sex
female
male
B GNG016 top inputs
Aversive cluster
Proportion of Total Inputs
Input type
C Feeding inhibition by the aversive cluster
Proportion GNG016 Input:
LgAG3 0.100
LB1e 0.098
LB1c 0.093
LB1b 0.071
LgAG5 0.031
PhG16 0.030
PhG14 0.025
PhG13 0.023
LB1a 0.015
GNG016
0.05
GNG510
GNG087 (Scapula)
Proboscis Extension
0.10
0.06
GNG088
Swallowing
Proportion GNG510 Input: 0.03 0.02 0.03 0.03
LB2c LB2b
LgAG7 LgAG9
D GNG055 top inputs
Proportion of Total Inputs
Input type
E Feeding inhibition by PhG2
GNG055
0.129
0.015
PhG2
0.053
0.015
LB1c
PRW055
0.035
GNG588 (Fdg)
Stopping
Proboscis positioning
F Multilayer inhibition of feeding
Aversive GRNs
Aversive high order
High order
MN
Attractive GRNs
Premotor
G AN05B023a top inputs
Proportion of Total Inputs
Input type
H Courtship inhibition
LgAG1
WG1
LgLG2
0.28
0.23
0.19
AN05B023a
0.019
AN05B102a (PPN1)
Intra-sex Courtship
Excitation (ACh)
Inhibition (GABA or Glut)
Promoting action
Inhibiting action

Figure 8

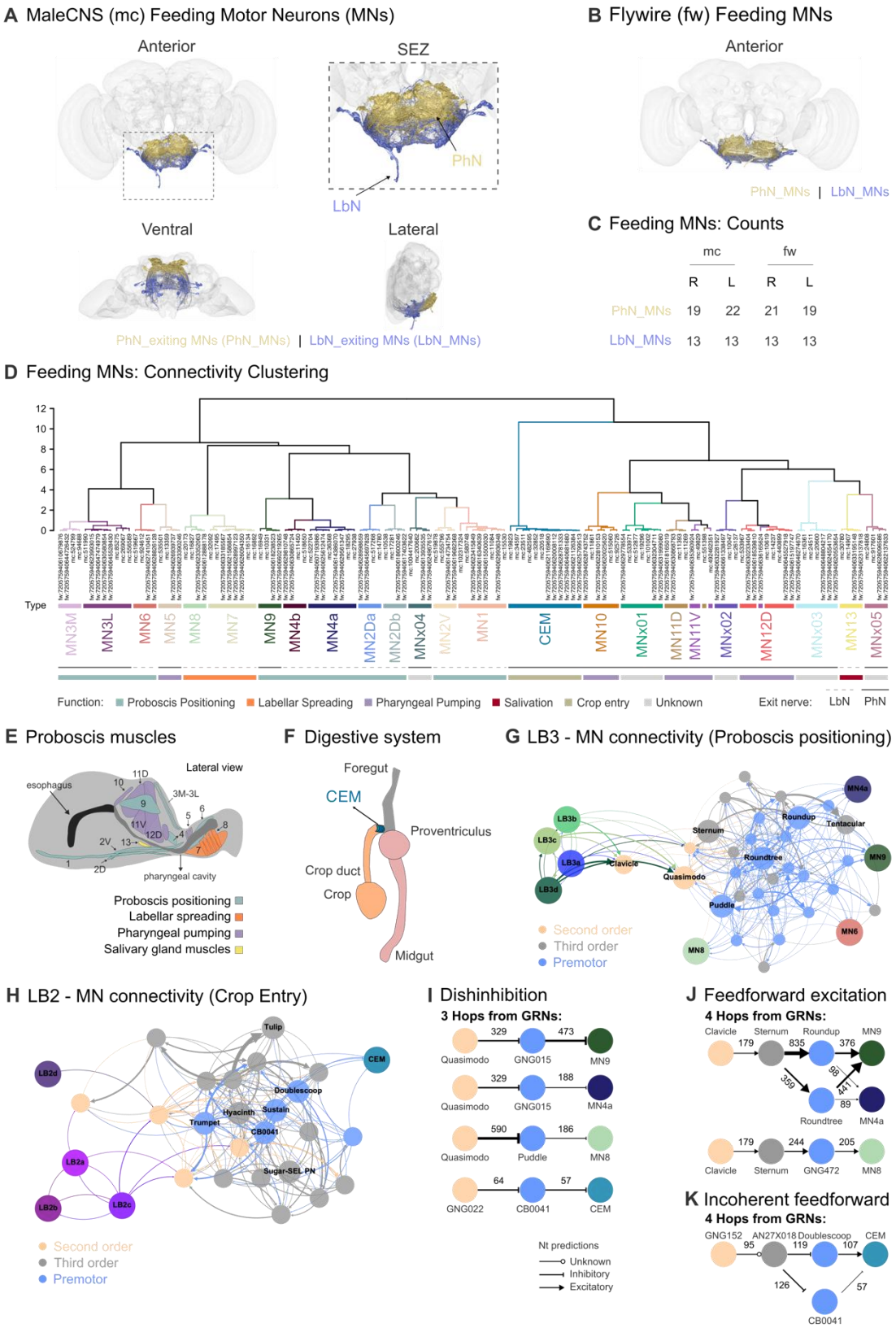
A MaleCNS (mc) Feeding Motor Neurons (MNs)
Anterior
SEZ
PhN
LbN
Ventral
Lateral
PhN_exiting MNs (PhN_MNs) | LbN_exiting MNs (LbN_MNs)
B Flywire (fw) Feeding MNs
Anterior
PhN_MNs | LbN_MNs
C Feeding MNs: Counts
mc fw
R L R L
PhN_MNs 19 22 21 19
LbN_MNs 13 13 13 13
D Feeding MNs: Connectivity Clustering
Type
MN3M MN3L MN6 MN5 MN8 MN7 MN9 MN4b MN4a MN2Da MN2Db MNx04 MN2V MN1 CEM MN10 MNx01 MN11D MN11V MNx02 MN12D MNx03 MN13 MNx05
Function: Proboscis Positioning Labellar Spreading Pharyngeal Pumping Salivation Crop entry Unknown
Exit nerve: LbN PhN
E Proboscis muscles
Lateral view
esophagus
pharyngeal cavity
Proboscis positioning
Labellar spreading
Pharyngeal pumping
Salivary gland muscles
F Digestive system
Foregut
CEM
Proventriculus
Crop duct
Crop
Midgut
G LB3 - MN connectivity (Proboscis positioning)
Second order
Third order
Premotor
H LB2 - MN connectivity (Crop Entry)
Tulip
CEM
Doublescoop
Hyacinth
Sustain
Trumpet
CB0041
Sugar-SEL PN
Second order
Third order
Premotor
I Dishinhibition
3 Hops from GRNs:
Quasimodo GNG015 MN9
Quasimodo GNG015 MN4a
Quasimodo Puddle MN8
GNG022 CB0041 CEM
Nt predictions
Unknown
Inhibitory
Excitatory
J Feedforward excitation
4 Hops from GRNs:
Clavicle Sternum Roundup MN9
Roundtree MN4a
Clavicle Sternum GNG472 MN8
K Incoherent feedforward
4 Hops from GRNs:
GNG152 AN27X018 Doublescoop CEM
CB0041

Figure 9

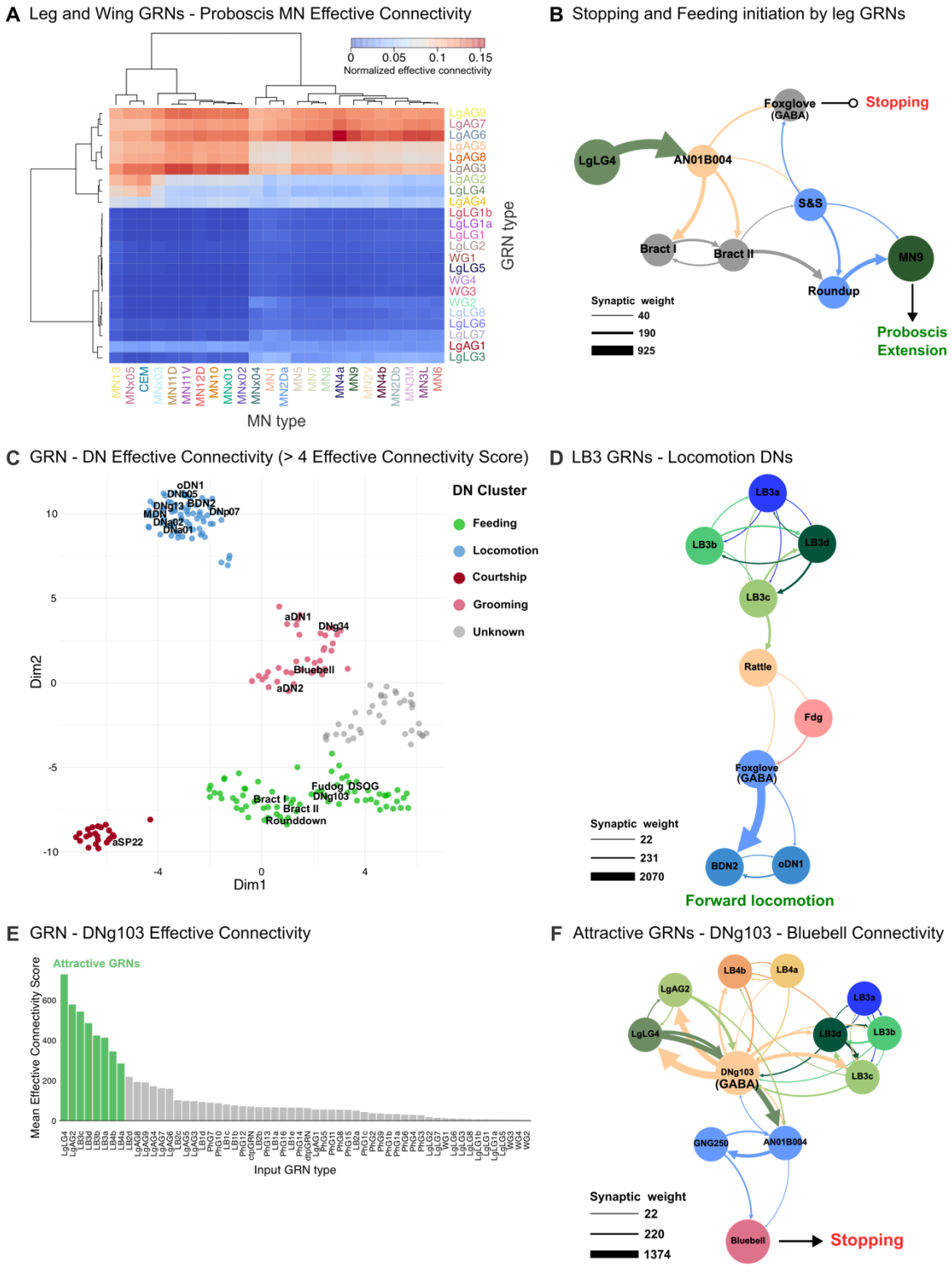
A Leg and Wing GRNs - Proboscis MN Effective Connectivity
0 0.05 0.1 0.15
Normalized effective connectivity
GRN type
MN type
B Stopping and Feeding initiation by leg GRNs
Foxglove (GABA)
Stopping
LgLG4
AN01B004
S&S
Bract I
Bract II
MN9
Roundup
Synaptic weight
40
190
925
Proboscis Extension
C GRN - DN Effective Connectivity (> 4 Effective Connectivity Score)
DN Cluster
Feeding
Locomotion
Courtship
Grooming
Unknown
Dim1
Dim2
aDN1
DNg34
Bluebell
aDN2
Fudog DSOG
DNg103
Bract I
Bract II
Roundown
aSP22
D LB3 GRNs - Locomotion DNs
LB3a
LB3b
LB3d
LB3c
Rattle
Fdg
Foxglove (GABA)
BDN2
oDN1
Synaptic weight
22
231
2070
Forward locomotion
E GRN - DNg103 Effective Connectivity
Attractive GRNs
Mean Effective Connectivity Score
Input GRN type
F Attractive GRNs - DNg103 - Bluebell Connectivity
LB4b
LB4a
LgAG2
LgLG4
LB3a
LB3d
LB3b
DNg103 (GABA)
LB3c
GNG250
AN01B004
Bluebell
Stopping
Synaptic weight
22
220
1374

Figure 10

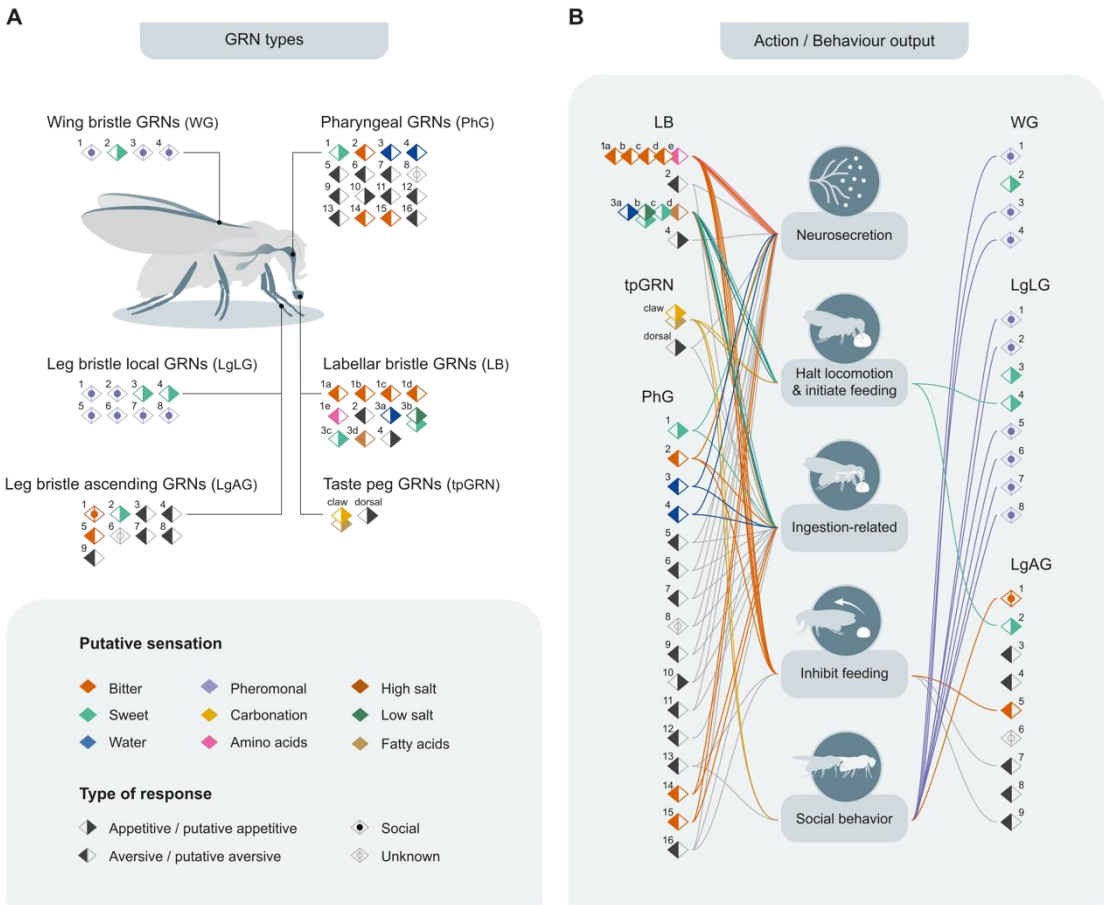
A
GRN types
Wing bristle GRNs (WG)
Pharyngeal GRNs (PhG)
Leg bristle local GRNs (LgLG)
Labellar bristle GRNs (LB)
Leg bristle ascending GRNs (LgAG)
Taste peg GRNs (tpGRN)
claw
dorsal
Putative sensation
Bitter
Sweet
Water
Pheromonal
Carbonation
Amino acids
High salt
Low salt
Fatty acids
Type of response
Appetitive / putative appetitive
Aversive / putative aversive
Social
Unknown
B
Action / Behaviour output
LB
tpGRN
PhG
WG
LgLG
LgAG
Neurosecretion
Halt locomotion
& initiate feeding
Ingestion-related
Inhibit feeding
Social behavior

Figure Legends

Figure 1. Characterization of *Drosophila melanogaster*'s gustatory system at the light level

A. Confocal images using the nuclear marker, UAS-RedStinger, to label GRNs housed in taste bristles in the anterior margin of the wings and on both the tarsi and tibia of all six legs. The membrane-tethered UAS-mCD8:GFP under the control of *poxn-GAL4* was used to label GRNs housed in three other body parts: taste bristle on the external surface of the labellum; taste pegs located between pseudotrachea on the inner surface of the labellum; taste pores, marked with an asterisk (*), across the pharynx, specifically, in the labral sensory organ (LSO), ventral cibarial sensory organ (VCSO) and dorsal cibarial sensory organ (DCSO). **B.** Expression of membrane-tethered mCD8:GFP under the control of the *Ir25a-* and *poxn-GAL4* driver is present in all GRN subclasses projecting, respectively, to the SEZ in the brain (right) and the VNC (left). The GRN axonal projections of each taste sensilla type are shown in a different color: labellar bristles in green; taste pegs in pink; pharyngeal sensilla in orange; leg bristles in blue and wing bristles in red. **C.** Rendering of all neurons identified per GRN subclass in maleCNS in three different views, anterior (right), ventral and lateral (left). Identification of the GRNs in the connectome were achieved by defining seed planes across their specific entry nerve: labial nerve (LbN) for labellar bristle (green) and taste peg (pink) GRNs; accessory pharyngeal nerve (aPhN) for LSO and VCSO pharyngeal GRNs (light orange); pharyngeal nerve (PhN) for DCSO pharyngeal GRNs (dark orange); prothoracic (ProLN), mesothoracic (MesoLN), metathoracic (MetaLN) leg nerves, respectively, for fore-, mid- and hindleg bristle GRNs (blue); anterior dorsal mesothoracic nerve (ADMN) for wing bristle GRNs. Leg bristle GRNs are subdivided into ascending, which project through the cervical connective (CV) and arborize in the SEZ and the local that terminate in the VNC. **D.** Ventral view of the renderings of the GRN subclasses – leg bristle ascending, leg bristle local and wing bristle GRNs – identified in MANC. **E.** Anterior view of the renderings of the GRN subclasses – labellar bristle, taste peg, pharyngeal and leg bristle ascending GRNs – identified in FAFB – FlyWire. **F.** GRN counts per subclass across the right (R) and left (L) sides for maleCNS, FAFB – FlyWire and MANC. A sexual dimorphism (SD) is found solely for the taste peg GRN counts. The difference in the counts of labellar bristle GRNs between maleCNS and FAFB – FlyWire have been linked to automated segmentation errors.

Figure 2. Cell typing the labellar bristle GRNs

A. Anterior view of the renderings of lbGRNs in maleCNS. **B.** Anterior view of the renderings of lbGRNs in FAFB – FlyWire. **C.** Anterior view of maleCNS and FAFB – FlyWire lbGRNs overlaid in maleCNS space, showing conversed broad anatomy of these neurons across different brains. **D.** Hierarchical co-clustering of maleCNS and FAFB – FlyWire lbGRNs based on outputs using cosine similarity and a threshold of 2 synapses. Color bars represent the type (top) and subtype (bottom) defined for each male and female lbGRN according to the connectivity clustering for maleCNS and FAFB – FlyWire neurons separately (Figures S1B and S1C). In contrast to LB3, LB1, LB2 and LB4 subtypes co-cluster together across the two connectomes. **E.** Anterior view of the renderings of lbGRNs per subtype across the right (R) and left (L) sides for maleCNS and FAFB – FlyWire, revealing their morphologies that are preserved between different brains. Presence of LB2d only in maleCNS is very likely not due to sexually dimorphism, but the result of technical difficulties due to automated segmentation. Outlined in red and green are the types we propose to be, respectively, aversive and appetitive. The putative sensations of each subtype are also indicated. The asterisk (*) indicates the subtypes for which we do not show a receptor-GAL4 match but infer from the literature. **F.** lbGRN counts per subtype across hemispheres within each connectome. The challenges faced while reconstructing the maleCNS lbGRNs have affected mostly the LB3a and LB3b subtypes. **G.** Substacks of confocal imaging for *Gr33a-, ppk28-* and *Gr64f-GAL4* positive lbGRNs were matched, respectively, to subtypes LB1a-d, LB3a and LB3b-c, suggesting they correspond to the bitter-, water- and sugar-sensing lbGRNs.

Figure 3. Cell typing the taste peg GRNs

A. Anterior view of the renderings of tpGRNs in maleCNS. **B.** Anterior view of the renderings of tpGRNs in FAFB – FlyWire. **C.** Anterior view of maleCNS and FAFB – FlyWire tpGRNs overlaid in maleCNS space. The overall anatomies are preserved, but inter-individual variabilities are highlighted via specific observable differences in the GRNs' projection fields between the two brains. **D.** Hierarchical co-clustering of maleCNS and FAFB – FlyWire tpGRNs based on outputs using cosine similarity and a threshold of 2 synapses, reveals two types, dorsal and claw tpGRNs, consistently to the connectivity clustering with solely the male and female tpGRNs[47] (Figure S2). **E.** Anterior view of the renderings of the morphologically distinct dorsal and claw tpGRNs across the two hemispheres within maleCNS and FAFB – FlyWire. Sparse anatomical variabilities between datasets within each

type do not translate in direct connectivity differences. **F.** tpGRN type counts per side across male and female demonstrates that the reported extra peg row in female flies houses claw tpGRNs. **G.** Substack of confocal scanning for *Gr5a-* and *Ir60d-GAL4* positive tpGRNs were matched specifically to the dorsal tpGRNs while *Ir56d-* and *Gr64e-GAL4* positive tpGRNs were matched to claw tpGRNs.

Figure 4. Cell typing the pharyngeal GRNs

A. Anterior view of phGRN renderings in maleCNS, showing its terminal arborizations in the SEZ. **B.** Anterior view of phGRN renderings in FAFB – FlyWire. **C.** Anterior view of maleCNS and FAFB – FlyWire phGRNs overlaid in maleCNS space, demonstrating the morphological preservation of this GRN subclass across brains. **D.** Hierarchical co-clustering of maleCNS and FAFB – FlyWire phGRNs based on outputs using cosine similarity and a threshold of 5 synapses. Each neuron is colored in accordance with its type (top) and subtype (bottom), the latter only applied to PhG1. Male and female neurons of the corresponding types cluster together (Figures S3B and S3C). **E.** Anterior view of renderings of aPhN- and PhN-projecting phGRN types, the latter corresponding to PhG7-9, reveal unique morphologies that are conserved between different brains. **F.** phGRN counts per side compared between maleCNS and FAFB – FlyWire shows a conservation per type and subtype across brains. **G.** Substack from confocal images of *Gr64e-, ppk28-, Ir67c-, Gr77a-* and *Ir60d-GAL4* positive phGRNs matched, respectively, to the PhG1, PhG3&4, PhG13, PhG15 and PhG16 types.

Figure 5. Cell typing the leg bristle ascending GRNs

A. Rendering of lgAGRNs in maleCNS in two different views, anterior and ventral, highlighting, respectively, the SEZ projections and axonal entry points in the VNC. **B.** Rendering of lgAGRNs in FAFB – FlyWire in an anterior view. In FAFB – Flywire, these neurons are restricted to their SEZ terminal arborizations. **C.** Anterior and ventral views of maleCNS and FAFB – FlyWire lgAGRNs overlaid in maleCNS space, revealing anatomical variabilities in their SEZ projections across the two connectomes (arrowhead). **D.** Hierarchical co-clustering of maleCNS and FAFB – FlyWire lgAGRNs based on outputs using cosine similarity and a threshold of 2 synapses. Each neuron is colored in accordance with its type, which was defined by connectivity clustering the male and female neurons separately (Figures S4B and S4C). **E.** Anterior view of each lgAGRN cell type, LgAG1-9, rendering across maleCNS and FAFB – FlyWire. Inter-individual morphological variabilities do not translate into direct downstream connectivity differences. **F.** LgAG1-9 counts per side are essentially consistent across the two connectomes. **G.** Substack of confocal image for *Gr33a-GAL4* lgAGRN positive population matches the LgAG1 type, suggesting a role in inhibiting conspecific male and interspecies courtship.

Figure 6. Cell typing the wing and leg bristle local GRNs

A. Ventral view of wGRN and lgLGRN renderings in maleCNS. While wGRNs arborize solely within T2 in the VNC, lgLGRNs project across all thoracic neuromeres depending on if housed in the fore-, mid- and hindleg taste bristles. **B.** Ventral view of wGRN and lgLGRN renderings in MANC. **C.** Hierarchical co-clustering of maleCNS and MANC wGRNs based on outputs using cosine similarity and a defined threshold of 2 synapses. Neurotransmitter predictions are indicated. **D.** Ventral view of each wGRN cell type, WG1-4, rendering across maleCNS and MANC. **E.** wGRN type counts per side, which are essentially the same between types, are consistent across both male connectomes. **F.** Ventral view of all maleCNS wGRN types overlaid to reveal their different projection fields in the neuropil. **G.** Hierarchical co-clustering of maleCNS and MANC foreleg local GRNs based on outputs using cosine similarity and a defined threshold of 2 synapses. The neurons are colored according to their type (left), LgLG1-8. LgLG1 type neurons are subtyped as LgLG1a and LgLG1b, depending on whether they are predicted to release acetylcholine or glutamate. The respective co-clusterings of mid- and hindleg LGRNs are found in Figures S5C and S5E. **H.** Ventral view of the renderings of lgLGRN types across maleCNS and MANC. LgLG1-4 span the T1-3 VNC segments while LgLG5-8 correspond exclusively to foreleg GRNs. **J.** Foreleg local GRN type counts per side are within the same range across the two connectomes.

Figure 7. Functional organization of the gustatory connectome

A. UMAP embedding of SEZ-projecting GRN types from maleCNS and FAFB – FlyWire datasets based on their downstream connectivity. Each GRN is colored by its type. The shapes represent sex. Circle: female (FlyWire), triangle: male (maleCNS). Key GRN types in each cluster were labeled. Different clusters are encircled with distinct colors. Aversive cluster (red), and attractive cluster (green) are labeled accordingly. Dim 1: Dimension 1, Dim 2: Dimension 2. **B.** Top GRN inputs to

second order neuron, GNG016 shown as proportions of total inputs to GNG016. Input GRN types that are found in the aversive cluster in **A** are colored (red). **C.** The sensorimotor pathway mediating feeding inhibition by the aversive cluster at different circuit levels. Each GRN type is colored. Red and yellow rectangles represent the aversive clusters in **A**. Each circle is a cell type. Synaptic weights are given as proportions of total inputs on downstream neurons. If a downstream cell type was previously identified in the literature, its name is indicated (e.g., Scapula). Otherwise maleCNS cell types are used. Scapula was proposed to inhibit feeding by inhibiting premotor neurons[45]. GNG088 is predicted to be GABAergic premotor neuron upstream of MNs controlling swallowing. **D.** Top inputs of GNG055 as described in **B**. GRN types are highlighted by their respective colors. **E.** A parallel pathway for feeding inhibition via PhG2 and LB1c. Synaptic weights are given as proportions of total inputs on downstream neurons. **F.** Circuit model for nested inhibition of feeding by diverse set of aversive GRN types. Feeding is inhibited at multiple circuit layers ranging from high order to premotor to motor neurons (See Figure S7). **G.** Top inputs of another second order neuron, AN05B023a as described in **B**. GRN types are highlighted by their respective colors. **H.** Candidate male – male courtship inhibition pathway by LgAG1 – AN05B023 – PPN1 pathway. Synaptic weights are given as proportions of total inputs on downstream neurons. A cell type is considered excitatory if it is predicted to be cholinergic (ACh), inhibitory if predicted to be GABAergic or glutamatergic.

Figure 8. Characterization of feeding motor outputs from the GRN cell types

A. Rendering of the feeding motor neurons in maleCNS in three different views, anterior, ventral and lateral, colored according to their exiting nerve, labial (LbN) or pharyngeal (PhN) nerve. The SEZ is highlighted to showcase the different projecting fields of the two neuronal populations. **B.** Rendering of the feeding motor neurons in FAFB – FlyWire in an anterior view. **C.** PhN- or LbN-exiting MN counts per side reveals comparable numbers between the two connectomes. **D.** Hierarchical co-clustering of the maleCNS and FAFB – FlyWire feeding MNs based on inputs using cosine similarity and a defined threshold of 5 synapses. Male and female MN corresponding types (Supplementary Figures 8B-C) cluster mostly together. When known, the MN type's general function is indicated as well as its exiting nerve. **E.** Lateral view of the fly's proboscis muscles, which are colored according to their general role, which can be controlling the proboscis' positioning (blue), involving either its extension or retraction, they can also mediate labellar spreading (orange), pharyngeal pumping (purple) or control salivation by innervating the salivary gland muscles (yellow). **F.** Schematic representation of the location of the muscles at the crop entrance that are innervated by CEM. **G.** The sensorimotor pathway connecting attractive lbGRN subtypes, LB3a-d, to feeding motor neurons controlling different steps of proboscis extension (MN9, MN4a, MN6 and MN8). The pathway is reconstructed by extracting cell types with high effective connectivity scores with both GRNs and MNs (>80th quantile) at each hop. Each circle is a cell type. Second order neurons are colored light orange. Premotor neurons are colored light blue. If a downstream cell type is previously studied or a driver line exists, its name is labeled. **H.** Same as **G** for the sensorimotor pathway connecting LB2 subtypes to crop entry motor neurons (CEMs). **I.** Disinhibition of feeding MNs by GABAergic second order neurons, Quasimodo and GNG022. Whether a neuron is inhibitory/excitatory is derived from neurotransmitter predictions as in **Figure 7**. Absolute synaptic weights are given. **J.** Same as **I** for feedforward excitation of feeding MNs. Clavicle is a key second order neuron mediating feedforward excitation. **K.** Incoherent feedforward loop connecting LB2s to CEMs. GNG152 is a key second order neuron, with low confidence neurotransmitter predictions (unknown sign for connection).

Figure 9. Control of different motor actions by different types of GRNs via ascending and descending pathways

A. Heatmap for effective connectivity from leg and wing GRNs to feeding motor neurons. Effective connectivity scores were normalized by the total effective connectivity to each MN. For effective connectivity calculations maximum seven hops were used. Ward's method was used for hierarchical clustering and building the dendrograms. **B.** LgLG4s downstream pathway mediates stopping and proboscis extension. If a downstream cell type is previously studied or a driver line exists, the name in the literature is used. Otherwise maleCNS cell types are used. Each circle is a cell type. Second order neurons are colored light orange. Premotor neurons are colored light blue. Absolute synaptic weights are given. **C.** UMAP embedding of DNs based on their effective connectivity scores with GRN types. Only DNs that have >4 effective connectivity score are shown. Each circle is a DN cell type, and each cluster is color coded. DNs studied previously and in this study are labeled. **D.** Attractive lbGRNs control locomotion. If a downstream cell type is previously studied or a driver line exists, the name in the literature is used. Otherwise maleCNS cell types are used. Each circle is a cell type. Absolute

synaptic weights are given. BD2 and oDN1 are two DN types that are shown to be involved in forward locomotion[76,96]. **E.** GRN – DNg103 effective connectivity. GRNs in the attractive cluster (**Figure 7**) are highlighted in green. **F.** Attractive GRNs and GABAergic DNg103 form a negative feedback loop to control Bluebell, of which activation leads to stopping[76,96], via AN01B004 and GNG250. Each circle is a cell type. Absolute synaptic weights are given. If a downstream cell type is previously studied or a driver line exists, the name in the literature is used. Absolute synaptic weights are given.

Figure 10. Summary of the fly gustatory connectome and its actions

A. Schematic summary of different GRN types across different body parts and their sensory profiles based on our predictions. The type of responses (appetitive, aversive or social), which we predict these GRN types are involved in, are also shown. Colors indicate putative sensation, and different shapes indicate the predicted responses mediated by GRN types. **B.** Actions and behavioral outputs mediated by different GRN types. Lines connect GRN types to actions we predict them to mediate. Most GRN types have a predicted sensation, valence (response) and action. Social behavior comprises sexual behaviors.

Figure S1. Cell typing the labellar bristle GRNs

A. Rendering of lbGRNs in maleCNS in two different views, ventral and lateral. **B.** Hierarchical clustering based on outputs of the lbGRNs identified in maleCNS using cosine similarity and a threshold of 2 synapses. The neurons were divided into four types, LB1-4, which were, in turn, subdivided into subtypes, respectively, LB1a-e, LB2a-d, LB3a-d and LB4a-b. **C.** Connectivity clustering of the FAFB – FlyWire lbGRNs performed in the same conditions as above. The same four lbGRN types were defined (top colored bars), LB1-4, each, further, subdivided into corresponding subtypes (bottom colored bars), respectively, LB1a-e, LB2a-c, LB3a-d and LB4a-b. **D.** Left: anterior view of renderings of each lbGRN type across maleCNS and FAFB – Flywire. Right: anterior view of the individual lbGRN type renderings overlaid for each connectome. **E.** Anterior view of the renderings of the LB3 and LB4 types in both connectomes to illustrate their different projection fields. **F.** Anterior view of the renderings of the LB1e subtype and the LB2 type overlaid in both connectomes to demonstrate their close morphologies, despite distinct direct downstream connectivity.

Figure S2. Cell typing the taste peg GRNs

A. Rendering of tpGRNs in maleCNS in two different views, ventral and lateral, to reveal their SEZ arborizations. **B.** Hierarchical clustering based on outputs of the tpGRNs identified in maleCNS using cosine similarity and a threshold of 2 synapses, reveals two different cell types (colored accordingly), which we named, dorsal and claw tpGRNs.

Figure S3. Cell typing the pharyngeal GRNs

A. Rendering of phGRNs in maleCNS in two different views, ventral and lateral, to reveal their SEZ projection pattern. **B.** Hierarchical clustering based on outputs of the phGRNs identified in maleCNS using cosine similarity and a threshold of 5 synapses. In different colors are the sixteen phGRN cell types, PhG1-16, and the three exclusively PhG1 subtypes, PhG1a-c. **C.** Connectivity clustering of the FAFB – FlyWire phGRNs performed in the same conditions as above, which resulted in the corresponding types, PhG1-16, and subtypes, PhG1a-c. **D.** Rendering of AN05B035, a potentially male-specific AN, which is one of the top downstream partners of the PhG13 type. The AN is shown in two distinct views: anterior (left) to highlight the AN's SEZ projections, especially, the branches that innervate the known sexually dimorphic region around the esophagus, and ventral (right) to reveal its arborization in the T1 segment of the VNC.

Figure S4. Cell typing the leg bristle ascending GRNs

A. Lateral view of the lgAGRN renderings in maleCNS. **B.** Hierarchical clustering based on outputs of the lgAGRNs identified in maleCNS using cosine similarity and a threshold of 2 synapses. In different colors are the nine lgAGRN cell types defined, LgAG1-9. **C.** Counts per side of each male LgAG type across the front-, mid- and hindlegs, which reveals that the types can be grouped into three categories, one including the types that span all legs, a second corresponding to mid- and hindleg exclusive types and a third of solely foreleg types. **D.** Connectivity clustering of the FAFB – FlyWire lgAGRNs done in the same conditions as above, resulting in the corresponding LgAG1-9 types.

Figure S5. Cell typing the wing and leg bristle local GRNs

A. Hierarchical clustering of the wGRNs identified in maleCNS based on their outputs. The clustering was done using cosine similarity and a threshold of 2 synapses. In different colors are the four wGRN types defined, WG1-4. The predicted neurotransmitter released by WG3 and WG4 GRNs, respectively, glutamate (Glut) and acetylcholine (ACH), is also indicated. **B.** Connectivity clustering of the MANC wGRNs using the same parameters as described above. The corresponding four types were defined. **C.** Co-clustering of the maleCNS and MANC midleg LGRNs performed under the conditions described before. Colored bars on top indicate the type, LgLG1-4, and the bottom ones the subtypes, LgLG1a-b. The latter were defined according to the predicted neurotransmitter release by each LgLG1 GRN, either ACH or Glut. **D.** Counts per side for each midleg LGRN type and subtype, when applicable, across maleCNS and MANC. **E.** Co-clustering of the maleCNS and MANC hindleg LGRNs as done for the midleg LGRN, resulting in the corresponding types, LgLG1-4, and subtypes, LgLG1a-b. **F.** Counts per side for each hindleg LGRN type and subtype, when applicable, in both connectomes. **G.** Ventral view of the overlay of the renderings of the maleCNS LgLG1-4. **H.** Ventral view of the overlay of the renderings of the maleCNS LgLG1 subtypes, LgLG1a-b, revealing overlapping projection fields.

Figure S6. Sexually dimorphic and male-specific downstream partners of VNC-projecting GRNs

A. Renderings of sexually dimorphic partners of wGRNs in maleCNS (left column, anterior and ventral views) and FAFB – FlyWire (right column, anterior view). maleCNS and FAFB – FlyWire cell types are indicated. Sexually dimorphic projections are highlighted with arrowheads. **B.** Male-specific or sexually dimorphic downstream partners of LgLG5-8 are rendered (left panels: anterior views, right panels: ventral views).

Figure S7. UMAP embedding of the appetitive and aversive clusters

A. and **B.** UMAP embedding of only **A.** aversive or **B.** attractive GRN types in maleCNS and FlyWire. Each GRN is colored by its type. The shapes represent sex. Circle: female (FlyWire), triangle: male (maleCNS).

Figure S8. Connectivity of key aversive downstream partners

A. Top output partners of GNG016 shown as proportions of its total outputs. GRN types are highlighted by their respective colors. GNG510 is highlighted as its top downstream interneuron. **B.** Top input partners of GNG510 are shown as proportion of its total inputs. GNG016 is highlighted as its top upstream partner. GRN types are highlighted by their respective colors. **C.** Top output partners of GNG510 shown as proportions of its total outputs. GNG087 and GNG088 are highlighted as its top downstream partners. **D.** Top input partners of GNG087 (Scapula) are shown as proportion of its total inputs. GNG510 is highlighted as its top upstream partner. GRN types are highlighted by their respective colors. **E.** Top input partners of GNG088 are shown as proportion of its total inputs. GNG510 is highlighted as its top upstream partner. **F.** GNG088 is a premotor neuron that is predicted to inhibit pharyngeal pumping motor neurons. Synaptic weights are given as the proportion of total inputs on the downstream MNs.

Figure S9. Cell typing of the feeding motor neurons

A. Hierarchical clustering of the feeding motor neurons (MNs) identified in maleCNS based on their inputs. The clustering was done using cosine similarity and a threshold of 5 synapses. In different colors are the defined MN types. **B.** Connectivity clustering of the FAFB – FlyWire feeding MNs using the same parameters as described above. In different colors are the corresponding MN types and, when existing, the FAFB – FlyWire cell type is also indicated. **C.** Rendering of each feeding MN type in either a ventral or an anterior view across maleCNS and FAFB – FlyWire. The MNs' exiting nerve is indicated with a dotted or a solid line, depending on if it is the labial or the pharyngeal nerve. The MNs are divided as proboscis positioning MNs, crop entry-controlling MN and the unknown ones, which to our knowledge have never been described in the literature. **D.** Counts per side for each feeding MN type in the two connectomes.

Figure S10. Proboscis muscles and their functions based on literature

The muscles involved in proboscis positioning and ingestion are highlighted. Rostrum: rostrum movements, haustellum: haustellum movements, labellum: labellar movements except labellar

abduction (spread). Labellar spread and pharyngeal pumping are grouped as ingestive processes. Functions are derived from[22,23]. Plus sign (+) indicates functionally characterized role. Minus sign (-) indicates the muscle is not involved in the movement. Asterisk (*) indicates proposed function based on the insertion site of the muscle.

Figure S11. Effective connectivity of labellar bristle GRNs to feeding motor neurons

A. Heatmap for mean effective connectivity scores from lbGRNs to feeding MN types in maleCNS (left panel) and FAFB – FlyWire (right panel). Maximum seven hops are used. Ward's method is used for hierarchical clustering and building the dendrograms. **B.** Effective connectivity of lbGRNs to MN types that control different steps of proboscis positioning, ingestion and crop entry across different hops (maximum 10 hops, see Reachability analysis in Methods.). Motor neurons and their roles are indicated.

Figure S12. Effective connectivity of taste peg and pharyngeal GRNs to feeding motor neurons

A. Heatmap for mean effective connectivity scores from tpGRNs to feeding MN types in maleCNS (left panel) and FAFB – FlyWire (right panel). Maximum seven hops are used. Ward's method is used for hierarchical clustering and building the dendrograms. **B.** Effective connectivity of tpGRNs to MN types that control different steps of proboscis positioning, ingestion and crop entry across different hops (maximum 10 hops). Motor neurons and their roles are indicated. **C.** Heatmap for mean effective connectivity scores from phGRNs to feeding MN types in maleCNS (left panel) and FAFB – FlyWire (right panel). Maximum seven hops are used. Ward's method is used for hierarchical clustering and building the dendrograms. **D.** Effective connectivity of phGRNs to MN types that control different steps of proboscis positioning, ingestion and crop entry across different hops (maximum 10 hops). Motor neurons and their roles are indicated.

Figure S13. Effective connectivity of GRN types with neurosecretory cells

A. Effective connectivity between GRN types and neurosecretory cell types plotted as a heatmap. Maximum seven hops are used. Ward's method was used for hierarchical clustering and building the dendrograms. **B.** The neural pathway between PhG1 subtypes and IPCs. Second order neurons are colored in light orange. Pre-IPC neurons are colored in light blue. If a downstream cell type is previously studied or a driver line exists, the name in the literature is used. Absolute synaptic weights are given in the legend.

Figure S14. Effective connectivity of leg bristle local GRNs with feeding motor neurons

A. Effective connectivity of lgLGRNs to MN types that control different steps of proboscis positioning, ingestion and crop entry across different hops (maximum 10 hops). Motor neurons and their roles are indicated. **B.** and **C.** The sensorimotor circuit that connects LgLG4 to **B.** pharyngeal pumping motor neuron MN11D and **C.** crop entry motor neuron CEM. maleCNS cell types are indicated. Absolute synaptic weights are given in the legend.

Figure S15. Effective connectivity of ctpGRNs with aSP22

A. Mean effective connectivity of each GRN type with courtship promoting descending neuron aSP22. ctpGRN, which has the highest score, is highlighted. **B.** The neural pathway that connects ctpGRN to aSP22 in three hops. Second order neurons are colored in light blue. Pre-DN neurons are colored in light blue. If a downstream cell type is previously studied or a driver line exists, the name in the literature is used. Absolute synaptic weights are given in the legend.